

Received 26 February 2024, accepted 5 March 2024, date of publication 7 March 2024, date of current version 28 March 2024.

Digital Object Identifier 10.1109/ACCESS.2024.3374776

RESEARCH ARTICLE

Remaining Useful Life Prediction for Two-Phase Hybrid Deteriorating Lithium-Ion Batteries Using Wiener Process

XUEMIAO CUI¹, JIPING LU^{1,2}, AND YAFENG HAN¹

¹School of Mechanical Engineering, Beijing Institute of Technology, Beijing 100081, China

²Changjiang Delta Institute, Beijing Institute of Technology, Jiaxing 314001, China

Corresponding author: Yafeng Han (hanyafeng@bit.edu.cn)

This work was supported in part by the Key Research and Development Programs of the Ministry of Science and Technology of China under Grant 2020YFB1712602.

ABSTRACT Owing to operating condition switching and internal degradation mechanisms, the degradation processes of some lithium-ion batteries (LIBs) exhibit non-monotone and two-phase patterns, which are composed of a linear first phase and a nonlinear second phase. The existing Gamma process and Inverse Gaussian process methods are limited to modeling the monotone degradation data. Besides, traditional single-phase nonlinear models and two-phase linear models are insufficient to describe such a degradation process effectively. Therefore, degradation modeling and remaining useful life (RUL) prediction of the hybrid deteriorating LIBs is still a compelling practical issue. In this paper, a two-phase hybrid degradation model with a linear first phase and a nonlinear second phase is formulated based on the widely used Wiener process-based model. Taking into account the random effects caused by the unit heterogeneity and the uncertainty of the degradation state at the changing point, we obtain the analytical solutions of the lifetime estimation and RUL prediction under the concept of the first passage time (FPT). In addition, to conduct model parameter identification, the expectation maximization (EM) algorithm in conjunction with a profile log-likelihood function method are utilized for offline parameter estimation. Subsequently, the Bayesian rule is adopted to conduct the online parameter updating. Finally, the numerical and practical experiments are provided for verification and show that the proposed method could achieve high estimation accuracy for the RUL prediction of the two-phase hybrid deteriorating LIBs.

INDEX TERMS Lithium-ion batteries, RUL prediction, two-phase degradation, unit-to-unit variability, Wiener process.

I. INTRODUCTION

In recent years, with the rapid development of technology, lithium-ion batteries (LIBs) have been widely used in many fields, including electric vehicles, large-scale grid, and aerospace power systems attributable to their high energy density, low self-discharge rate and long service life [1], [2], [3]. Despite the advantages, LIBs' performance will decrease gradually over time owing to the influence of dynamic environments and internal mechanisms [4], [5]. Degradation of LIBs will lead to equipment failure or even catastrophic

eventualities [6], [7], [8]. Hence, prognostics and health management (PHM) are essential for maintaining high efficiency and safe operation of LIBs [9]. Establishing suitable models to characterize the degradation process and realizing accurate remaining useful life (RUL) prediction are critical challenges of LIBs' PHM [10], [11], [12].

Generally, the RUL prediction approaches for LIBs can be classified into model-based and data-driven [13], [14]. At present, the data-driven approaches have become research hotspots in RUL prediction, as they exclusively rely on the performance data collected by sensors and do not require much knowledge about the physical and chemical mechanism of LIBs [15], [16]. The data-driven approaches mainly consist

The associate editor coordinating the review of this manuscript and approving it for publication was Jiajie Fan¹.

of machine learning and statistical approaches [17]. Machine learning methods such as neural networks and deep learning require massive data to obtain high-quality training feature variables and will generate cumulative errors [18]. In contrast, the statistical approaches attempt to combine the statistical models with degradation data, which can effectively capture the uncertainty of the degradation process [19]. As one widely used category of statistical approaches, stochastic process-based methods can characterize the randomness of the degradation process, provide the probability distribution of RUL, and quantify the prediction uncertainty [20], [21]. Wiener process, Gamma process, and Inverse Gaussian process are three commonly used stochastic process models [22]. Among them, the Wiener process model has attracted significant attention owing to its good mathematical properties in describing the non-monotone degradation trajectory [23], [24], [25]. As to the Wiener process-based degradation modeling method, the lifetime and RUL are usually defined as the first passage time (FPT) when the degradation process exceeds the preset failure threshold [26]. Since the degradation increments follow the normal distribution, the linear Wiener process is flexible in solving the analytical solutions of lifetime and RUL based on the FPT concept and has been extensively investigated over the last few decades [27], [28], [29]. However, for nonlinear degradation devices such as LIBs, nonlinearity is an important factor that cannot be ignored in degradation modeling. To characterize the nonlinear degradation process, Si et al. [30] first proposed a general nonlinear degradation model and obtained the probability density function (PDF) of RUL based on a well-known time-space transformation. After this pioneering work, extensive research has been conducted on the RUL prediction of nonlinear degradation devices [31], [32], [33], [34].

It is noticeable that the aforementioned Wiener process-based RUL prediction methods primarily focus on single-phase degradation cases. However, in practice, owing to operation conditions switching and inner degrading mechanisms evolution, the degradation rate of many batteries' degradation trajectories changes significantly and exhibits obvious two-phase characteristics [35], [36]. Hence, it is necessary to formulate a two-phase degradation model for accurate lifetime estimation and RUL prediction. Over the last few years, many advances have been made in the two-phase Wiener process-based degradation modeling method. Kong et al. [37] proposed a change-point Wiener process model to describe the two-phase degradation trajectory with abrupt jumps at the changing point and conducted the system reliability assessments. Based on the two-phase Wiener process, Zhang et al. [36] established a generalized degradation model framework for LIBs, then derived the analytical expressions of lifetime and RUL distribution under the concept of FPT. Gao et al. [38] constructed a two-phase Wiener process model with a changing point to analyze the degradation process of systems affected by shocks. To facilitate the degradation analysis of LIBs, Chen et al. [39]

proposed an adaptive RUL prediction method combining the two-phase linear Wiener model and the extreme learning machine algorithm.

However, most of the current researches only focus on the two-phase linear model, which may not be accurate in some complex LIBs applications. It is encountered in practice that some LIBs with two-phase degradation patterns exhibit a slow and stable linear trend in the first degradation phase while a fluctuating nonlinear trend in the subsequent degradation phase [40], [41], [42]. From a practical perspective, the reason for this phenomenon is that the internal active material of LIBs will gradually lose during cycling, whereas the internal resistance increases slowly [43]. When a certain number of cycles is reached, the capacity of the batteries will rapidly decrease, leading to nonlinear and non-monotone degradation characteristics. Obviously, if the two-phase linear model is still utilized for modeling, it will be difficult to describe the nonlinear degradation features of the second phase accurately, which may lead to estimate bias. Thus, determining how to model the two-phase degradation process of such LIBs is a compelling practical problem. However, only a few works refer to this issue [44], [45]. Shen et al. [44] established a change-point Wiener and Inverse Gaussian process model to characterize the two-phase degradation process of the revolute joints. In this work, the first phase was described by a linear Wiener process model, and the second phase with accelerated nonlinear features was captured by an Inverse Gaussian process model. It is noteworthy that the Inverse Gaussian process is limited to modeling the monotone degenerate trajectories. Thus, the above methods for mechanical devices are not suitable for LIBs degradation modeling. Fortunately, the nonlinear Wiener process can effectively characterize the nonlinearity of the non-monotone degradation process and could be used to derive the analytical form of lifetime estimation under the FPT concept [23], [46]. Therefore, it is more appropriate to utilize the linear Wiener process in conjunction with the nonlinear Wiener process to describe the two-phase degradation paths of the aforementioned LIBs.

To achieve accurate degradation modeling and RUL prediction for LIBs, several issues still need to be further investigated. Previous studies generally assumed that the occurring time of the changing point and its corresponding degradation state (i.e., the initial value of the second phase) are known or their distributions could be obtained through the statistical analysis of numerous degradation data [47], [48], [49]. Therefore, the randomness of the degradation state at the changing point is neglected, which may lead to estimate bias. In fact, due to the uncertainty of the first phase, the degradation state at the changing point is a random variable before the changing point appears, which is related to the degradation rate of the first phase and the changing time [50]. In addition, due to the influence of internal and external factors, unit heterogeneities exist in the degradation process of LIBs within the same batch. Thus, it is more reasonable to set the changing point and the degradation rates as random

variables [51], [52]. Hence, characterizing the unit-to-unit variability for the LIBs of the same specification based on real-time monitoring data to increase the adaptability of the degradation model is necessary. To the best of our knowledge, very limited work is available to solve the degradation modeling and RUL prediction problems for the two-phase hybrid deteriorating LIBs with a linear first phase and a nonlinear second phase in the existing literature, especially for the situation where all the above issues are considered at the same time.

Therefore, in this paper, a novel degradation modeling and RUL prediction strategy based on the Wiener process is proposed for two-phase hybrid deteriorating LIBs to bridge the aforementioned research gaps. The main contribution of this work lies in the following aspects.

1) A two-phase hybrid degradation model based on the Wiener process is established to characterize the degradation process of LIBs with a linear first phase and a nonlinear second phase.

2) The analytical solutions for the lifetime and RUL estimation considering the unit-to-unit variability and the random degradation state at the changing point are derived based on the FPT concept.

3) The offline parameter estimation is conducted by the EM algorithm in conjunction with a profile log-likelihood function method, and then the online parameter updating is realized by the Bayesian rule.

4) The effectiveness of the proposed method is verified based on the experiments of a numerical simulation and a practical case study of the LIBs degradation dataset.

The remainder of this paper is arranged as follows. Section II establishes a two-phase hybrid degradation model of LIBs, and derives the analytical solutions of the RUL estimation, then conducts the model parameter identification. The implementation details of the experiments are provided in Section III. Section IV presents the experimental results and analysis. Section V concludes this paper.

II. METHODOLOGY

In this section, the degradation modeling and RUL prediction methods of the two-phase hybrid deteriorating LIBs are introduced. The proposed methodology could be split into three major parts, namely the formulation of the degradation model, the derivation of the lifetime and RUL distribution under different conditions, and the model parameter identification. The details are described below.

A. MOTIVATION AND MODELING DESCRIPTION

Fig. 1 shows the capacity degradation data of five LIBs adopted from the Stanford University battery dataset [53]. It is observable from Fig. 1 that the degradation trajectories exhibit obvious two-phase hybrid deteriorating features with evident inflection points. Specifically, the LIBs' capacity decreases slowly in the first phase with a linear trend, and after about 500 cycles, the power starts to dive rapidly and show a nonlinear trend, which was disclosed by [41].

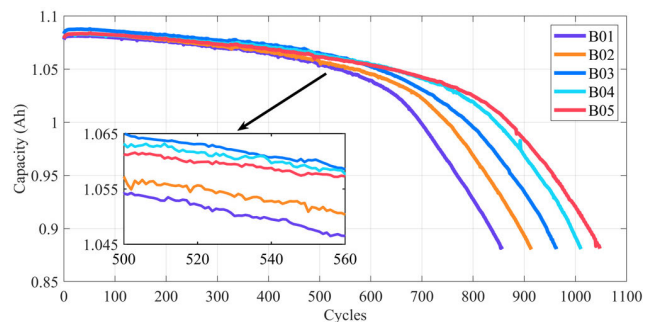


FIGURE 1. Degradation trajectories of batteries.

Furthermore, it is clear from Fig. 1 that the degradation trajectories are non-monotone. In this case, the degradation process could not be described well by the two-phase linear model. Therefore, it is appropriate to model the degradation process of such hybrid deteriorating LIBs based on the two-phase hybrid degradation model with a linear first phase and a nonlinear second phase.

It is known that among the stochastic process models, the Gamma process and Inverse Gaussian process are limited to modeling the monotone degenerate trajectory. However, the degradation trajectories of the LIBs' capacity in Fig. 1 are non-monotone. Therefore, the Gamma process-based methods and the Gaussian process-based methods in the existing literature are insufficient to model the LIBs' capacity degradation data.

Fortunately, the Wiener process has good mathematical properties in describing the non-monotone degradation trajectory. Thus, the Wiener process is employed in this paper to describe the degradation process of the hybrid deteriorating LIBs. For detail, the linear first phase of the LIBs degradation data could be modeled by the linear Wiener process. Besides, considering the nonlinear characteristics of the second phase, we adopt the nonlinear Wiener process model to describe its degradation features. The nonlinear Wiener process is a type of diffusion process with a nonlinear drift term, which is driven by the standard Brownian motion. The standard Brownian motion is a Gaussian process with a mean of 0 and a time-dependent variance, which is originally used to describe random walks of tiny particles [30]. Therefore, the nonlinear Wiener process is generally used to model the non-monotone degradation process with the nonlinear trend.

Inspired by the single-phase nonlinear degradation model discussed in [30] and [32] and the two-phase linear degradation model presented by [36], a two-phase hybrid degradation model consisting of a linear first phase and a nonlinear second phase can be formulated as follows,

$$X(t) = \begin{cases} x_0 + \lambda_1 t + \sigma_1 B(t), & 0 < t \leq \tau \\ x_\tau + \lambda_2 \int_\tau^t \mu(\rho - \tau; \vartheta) d\rho + \sigma_2 B(t - \tau), & t > \tau \end{cases} \quad (1)$$

where $X(t)$ denotes the degradation state at time t , τ represents the changing time. Thus, the degradation process is

divided into two parts by the changing point τ . The time from t_0 to τ is the first phase, whereas the time from τ to t represents the second phase. Therefore, $x_0 = 0$ is the initial value of the first phase, and x_τ is the degradation state at the changing time τ , as well as the initial value of the second phase. Besides, λ_1 and σ_1 represent the drift and diffusion coefficients of the first phase. $\lambda_2 \int_\tau^t \mu(\rho - \tau; \vartheta) d\rho$ and σ_2 represent the drift function and diffusion coefficient of the second phase. λ_2 is a proportional parameter that controls the speed of the nonlinear degradation (i.e., drift rate of the second phase), $\mu(t - \tau; \vartheta)$ is a nonlinear function with time t and an unknown parameter ϑ , which describes the nonlinear characteristics of LIBs. $B(t)$ denotes the standard Brown motion. For simplicity, the two-phase hybrid degradation model proposed in Equation (1) is referred to as THDM, and it is assumed that the two phases are independent of each other.

Generally, according to the concept of FPT, the lifetime T of the deteriorating LIBs described in Equation (1) can be defined as:

$$T = \inf \{t : X(t) \geq w | X(0) \leq w\} \quad (2)$$

where w is a predefined failure threshold determined by the relevant standards or engineering practice. Then, similar to the definition of the lifetime, the expression of RUL at the current time t_k can be defined as:

$$L_k = \inf \{l_k : X(t_k + l_k) \geq w | X(t_k) \leq w\} \quad (3)$$

where l_k is the time from t_k to the failure time, and L_k denotes the RUL with PDF $f_L(l_k)$.

B. RUL PREDICTION UNDER THE CONCEPT OF FPT

1) DERIVATION OF THE LIFETIME DISTRIBUTION BASED ON THDM WITH DETERMINISTIC PARAMETERS

Firstly, if the changing time is fixed, and all parameters in Equation (1) are known constant values, the lifetime distribution based on THDM is derived without considering the randomness of the parameters. Based on the research in [30], [32], and [36], the PDF of the lifetime T for the two-phase hybrid deteriorating LIBs can be formulated as follows,

(1) if $0 < t \leq \tau$

$$f_T(t|\lambda_1) = \frac{w - x_0}{\sqrt{2\pi\sigma_1^2 t^3}} \exp \left[-\frac{(w - x_0 - \lambda_1 t)^2}{2\sigma_1^2 t} \right] \quad (4)$$

(2) if $t > \tau$

$$f_T(t|\lambda_2, x_\tau) \cong \frac{w - x_\tau - \lambda_2 \left(\int_\tau^t \mu(\rho - \tau; \vartheta) d\rho - (t - \tau)\mu(t - \tau; \vartheta) \right)}{\sigma_2 \sqrt{2\pi(t - \tau)^3}} \times \exp \left[-\frac{\left(w - x_\tau - \lambda_2 \int_\tau^t \mu(\rho - \tau; \vartheta) d\rho \right)^2}{2\sigma_2^2(t - \tau)} \right] \quad (5)$$

2) LIFETIME ESTIMATION AND RUL PREDICTION BASED ON THDM WITH RANDOM EFFECT

In practical engineering, the degradation paths of different LIBs from the same batch have heterogeneity, which is called unit-to-unit variability. Generally, the individual features of different devices are described by random parameters in the degradation model [52]. However, the parameters in Equations (4) and (5) are deterministic. Therefore, to describe the unit-to-unit variability, a common method is assuming the drift coefficient of the first phase and the drift rate of the second phase in the THDM are random variables that follow the normal distribution, i.e., $\lambda_1 \sim N(\lambda_{1r}, \sigma_{1r}^2)$, $\lambda_2 \sim N(\lambda_{2r}, \sigma_{2r}^2)$. Based on the prior information obtained from historical data, the model parameters of a certain operating battery can be updated through real-time observations. Hence, when the changing time τ is fixed and known, the PDF of the lifetime T based on the THDM with unit-to-unit variability can be obtained as follows,

(1) if $0 < t \leq \tau$

$$f_T(t) = \int_{-\infty}^{+\infty} f_T(t|\lambda_1)p(\lambda_1)d\lambda_1 = \frac{w - x_0}{\sqrt{2\pi t^2(t^2\sigma_{1r}^2 + \sigma_1^2 t)}} \exp \left[-\frac{(w - x_0 - \lambda_{1r}t)^2}{2(t^2\sigma_{1r}^2 + \sigma_1^2 t)} \right] \quad (6)$$

(2) if $t > \tau$

$$f_T(t|x_\tau) = \int_{-\infty}^{+\infty} f_T(t|\lambda_2, x_\tau)p(\lambda_2)d\lambda_2 \cong \frac{1}{\sqrt{2\pi(t - \tau)^2 \left[\sigma_{2r}^2 \left(\int_\tau^t \mu(\rho - \tau; \vartheta) d\rho \right)^2 + \sigma_2^2(t - \tau) \right]^3}} \times \left[(w - x_\tau) \left(\sigma_{2r}^2 \left(\int_\tau^t \mu(\rho - \tau; \vartheta) d\rho \right)^2 + \sigma_2^2(t - \tau) \right) - \left(\int_\tau^t \mu(\rho - \tau; \vartheta) d\rho - (t - \tau)\mu(t - \tau; \vartheta) \right) \times \left((w - x_\tau)\sigma_{2r}^2 \int_\tau^t \mu(\rho - \tau; \vartheta) d\rho + \lambda_{2r}\sigma_2^2(t - \tau) \right) \right] \times \exp \left[-\frac{\left(w - x_\tau - \lambda_{2r} \int_\tau^t \mu(\rho - \tau; \vartheta) d\rho \right)^2}{2 \left(\sigma_{2r}^2 \left(\int_\tau^t \mu(\rho - \tau; \vartheta) d\rho \right)^2 + \sigma_2^2(t - \tau) \right)} \right] \quad (7)$$

Proof: See Appendix A.

To facilitate calculation, the above-presented results assume that the degradation state at the changing point is determined and known. In fact, if the changing point does not appear, the value of x_τ should be a random variable rather than a fixed value. According to the concept of FPT, the premise for the degradation process to enter the second phase is that

the battery has not failed in the first phase. That is to say, the degradation path does not reach the failure threshold w before the changing point appears. Therefore, to obtain the PDF of the lifetime T at the second phase, the transition probability density from x_0 to x_τ should be derived first. It is defined that $h_\tau(x_\tau) = \Pr\{X(\tau) = x_\tau | X(0) = x_0, T > \tau\} \Pr\{T > \tau\}$ denotes the transition probability function. After obtaining the analytic form of $h_\tau(x_\tau)$, the PDF of lifetime T could be derived based on the law of total probability.

According to the properties of the Wiener process, x_τ follows the normal distribution, i.e., $x_\tau \sim N(\lambda_1\tau, \sigma_1^2\tau)$. In addition, x_τ is determined by the drift and diffusion coefficients of the first phase, as well as the changing time.

Hence, to derive the analytic form of $h_\tau(x_\tau)$, Lemma 1 is introduced according to [54].

Lemma 1: If $X(t) = x_0 + \lambda_a t + \sigma_a B(t)$ represents a linear Brownian motion with $x_0 = 0$. Under an absorbing boundary w , the transition probability density of the state from x_0 to x during time t could be expressed as follows,

$$h(x, t) = \frac{1}{\sqrt{2\pi t\sigma_a^2}} \left\{ \exp\left[-\frac{(x - \lambda_a t)^2}{2\sigma_a^2 t}\right] - \exp\left(\frac{2\lambda_a w}{\sigma_a^2}\right) \exp\left[-\frac{(x - 2w - \lambda_a t)^2}{2\sigma_a^2 t}\right] \right\} \quad (8)$$

Then, the analytical form of $h_\tau(x_\tau)$ could be obtained based on Lemma 1, as follows,

$$h_\tau(x_\tau) = \frac{1}{\sqrt{2\pi\tau\sigma_1^2}} \left\{ \exp\left[-\frac{(x_\tau - \lambda_1\tau)^2}{2\sigma_1^2\tau}\right] - \exp\left(\frac{2\lambda_1 w}{\sigma_1^2}\right) \exp\left[-\frac{(x_\tau - 2w - \lambda_1\tau)^2}{2\sigma_1^2\tau}\right] \right\} \quad (9)$$

It is noted that $h_\tau(x_\tau)$ will change due to the randomness of the first phase model. Considering $\lambda_1 \sim N(\lambda_{1r}, \sigma_{1r}^2)$, $h_\tau(x_\tau)$ should be rewritten as $\int_{-\infty}^{+\infty} h_\tau(x_\tau | \lambda_1) p(\lambda_1) d\lambda_1$. Thus, based on Lemma 2 in Appendix A, the analytic form of $h_\tau(x_\tau)$ could be obtained [36].

$$h_\tau(x_\tau | \lambda_{1r}, \sigma_{1r}) = \frac{\exp\left[-\frac{(x_\tau - \lambda_{1r}\tau)^2}{2(\tau\sigma_1^2 + \tau^2\sigma_{1r}^2)}\right]}{\sqrt{2\pi(\tau\sigma_1^2 + \tau^2\sigma_{1r}^2)}} - \frac{\exp\left(\frac{2\lambda_{1r}w}{\sigma_1^2} + \frac{2(w^2\sigma_{1r}^4\tau + w^2\sigma_{1r}^2\sigma_1^2)}{(\sigma_1^2 + \tau\sigma_{1r}^2)\sigma_1^4}\right)}{\sqrt{2\pi(\tau\sigma_1^2 + \tau^2\sigma_{1r}^2)}} \times \exp\left[-\frac{\left(x_\tau - 2w - \lambda_{1r}\tau - \frac{2w\sigma_{1r}^2\tau}{\sigma_1^2}\right)^2}{2(\tau\sigma_1^2 + \tau^2\sigma_{1r}^2)}\right] \quad (10)$$

Then, if λ_1 and λ_2 follow the normal distribution, i.e., $\lambda_1 \sim N(\lambda_{1r}, \sigma_{1r}^2)$, $\lambda_2 \sim N(\lambda_{2r}, \sigma_{2r}^2)$, the PDF of the lifetime

T based on the THDM considering unit-to-unit variability and the randomness of x_τ with a certain changing time τ can be expressed as follows.

(1) When $0 < t \leq \tau$, the PDF of the lifetime T has been formulated in Equation (6).

(2) When $t > \tau$, the lifetime distribution could be obtained based on Equations (7) and (10),

$$f_T(t) \cong \int_{-\infty}^w f_T(t|x_\tau) h_\tau(x_\tau | \lambda_{1r}, \sigma_{1r}) dx_\tau \cong Q - R \quad (11)$$

where $Q = Q_1 - Q_2$, $R = R_1 - R_2$, and

$$Q_1 = \sqrt{\frac{r_{a1}^2}{2\pi(t - \tau)^2(\sigma_{\alpha 1}^2 + \sigma_{\beta 1}^2)}} \exp\left[-\frac{(\lambda_{\alpha 1} - \lambda_{\beta 1})^2}{2(\sigma_{\alpha 1}^2 + \sigma_{\beta 1}^2)}\right] \times \left\{ \frac{\lambda_{\beta 1}\sigma_{\alpha 1}^2 + \lambda_{\alpha 1}\sigma_{\beta 1}^2}{\sigma_{\alpha 1}^2 + \sigma_{\beta 1}^2} \times \Phi\left(\frac{\lambda_{\beta 1}\sigma_{\alpha 1}^2 + \lambda_{\alpha 1}\sigma_{\beta 1}^2}{\sqrt{\sigma_{\alpha 1}^2\sigma_{\beta 1}^2(\sigma_{\alpha 1}^2 + \sigma_{\beta 1}^2)}}\right) + \frac{\sigma_{\alpha 1}^2\sigma_{\beta 1}^2}{\sigma_{\alpha 1}^2 + \sigma_{\beta 1}^2} \times \phi\left(\frac{\lambda_{\beta 1}\sigma_{\alpha 1}^2 + \lambda_{\alpha 1}\sigma_{\beta 1}^2}{\sqrt{\sigma_{\alpha 1}^2\sigma_{\beta 1}^2(\sigma_{\alpha 1}^2 + \sigma_{\beta 1}^2)}}\right) \right\}$$

$$Q_2 = \sqrt{\frac{r_{b1}^2}{2\pi(t - \tau)^2(\sigma_{\alpha 1}^2 + \sigma_{\beta 1}^2)}} \exp\left[-\frac{(\lambda_{\alpha 1} - \lambda_{\beta 1})^2}{2(\sigma_{\alpha 1}^2 + \sigma_{\beta 1}^2)}\right] \times \left\{ 1 - \Phi\left(-\frac{\lambda_{\beta 1}\sigma_{\alpha 1}^2 + \lambda_{\alpha 1}\sigma_{\beta 1}^2}{\sqrt{\sigma_{\alpha 1}^2\sigma_{\beta 1}^2(\sigma_{\alpha 1}^2 + \sigma_{\beta 1}^2)}}\right) \right\}$$

$$R_1 = I_1 \times \sqrt{\frac{r_{a1}^2}{2\pi(t - \tau)^2(\sigma_{\alpha 1}^2 + \sigma_{\beta 1}^2)}} \exp\left[-\frac{(\lambda_{\alpha 1} - \lambda_{\gamma 1})^2}{2(\sigma_{\alpha 1}^2 + \sigma_{\beta 1}^2)}\right] \times \left\{ \frac{\lambda_{\gamma 1}\sigma_{\alpha 1}^2 + \lambda_{\alpha 1}\sigma_{\beta 1}^2}{\sigma_{\alpha 1}^2 + \sigma_{\beta 1}^2} \times \Phi\left(\frac{\lambda_{\gamma 1}\sigma_{\alpha 1}^2 + \lambda_{\alpha 1}\sigma_{\beta 1}^2}{\sqrt{\sigma_{\alpha 1}^2\sigma_{\beta 1}^2(\sigma_{\alpha 1}^2 + \sigma_{\beta 1}^2)}}\right) + \frac{\sigma_{\alpha 1}^2\sigma_{\beta 1}^2}{\sigma_{\alpha 1}^2 + \sigma_{\beta 1}^2} \times \phi\left(\frac{\lambda_{\gamma 1}\sigma_{\alpha 1}^2 + \lambda_{\alpha 1}\sigma_{\beta 1}^2}{\sqrt{\sigma_{\alpha 1}^2\sigma_{\beta 1}^2(\sigma_{\alpha 1}^2 + \sigma_{\beta 1}^2)}}\right) \right\}$$

$$R_2 = I_1 \times \sqrt{\frac{r_{b1}^2}{2\pi(t - \tau)^2(\sigma_{\alpha 1}^2 + \sigma_{\beta 1}^2)}} \exp\left[-\frac{(\lambda_{\alpha 1} - \lambda_{\gamma 1})^2}{2(\sigma_{\alpha 1}^2 + \sigma_{\beta 1}^2)}\right] \times \left\{ 1 - \Phi\left(-\frac{\lambda_{\gamma 1}\sigma_{\alpha 1}^2 + \lambda_{\alpha 1}\sigma_{\beta 1}^2}{\sqrt{\sigma_{\alpha 1}^2\sigma_{\beta 1}^2(\sigma_{\alpha 1}^2 + \sigma_{\beta 1}^2)}}\right) \right\}$$

$$\lambda_{\alpha 1} = \lambda_{2r} \left(\int_{\tau}^t \mu(\rho - \tau; \vartheta) d\rho \right), \lambda_{\beta 1} = w - \lambda_{1r}\tau,$$

$$\lambda_{\gamma 1} = -w - \lambda_{1r}\tau - \frac{2w\sigma_{1r}^2\tau}{\sigma_1^2},$$

$$\sigma_{\alpha 1}^2 = \sigma_{2r}^2 \left(\int_{\tau}^t \mu(\rho - \tau; \vartheta) d\rho \right)^2 + \sigma_2^2(t - \tau),$$

$$\sigma_{\beta 1}^2 = \tau\sigma_1^2 + \tau^2\sigma_{1r}^2,$$

$$\begin{aligned}
 r_{a1} &= \frac{(t - \tau) \left(\sigma_2^2 + \sigma_{2r}^2 \mu(t - \tau; \vartheta) \int_{\tau}^t \mu(\rho - \tau; \vartheta) d\rho \right)}{\sigma_{\alpha 1}^2}, \\
 r_{b1} &= \frac{(t - \tau) \sigma_2^2 (\lambda_{\alpha 1} - \lambda_{2r}(t - \tau) \mu(t - \tau; \vartheta))}{\sigma_{\alpha 1}^2}, \\
 I_1 &= \exp \left(\frac{2\lambda_{1r}w}{\sigma_1^2} + \frac{2(w^2\sigma_{1r}^4\tau + w^2\sigma_{1r}^2\sigma_1^2)}{(\sigma_1^2 + \tau\sigma_{1r}^2)\sigma_1^4} \right) \quad (12)
 \end{aligned}$$

It is worth mentioning that $\Phi(\cdot)$ and $\phi(\cdot)$ represent the cumulative distribution function (CDF) and PDF of the standard normal distribution, respectively.

Proof: See Appendix B

It is noticeable that the above-presented lifetime estimation equations are formulated for the whole degradation process of the battery from time t_0 to the FPT of the degradation path. However, if the current time is t_k , we need to further conduct the RUL prediction of the battery. It is known that at time t_k , the RUL of the battery is related to the actual degradation state $X(t_k)$. In such case, if t represents the FPT of the degradation process $\{X(t), t \geq t_k\}$, then the residual $t - t_k$ corresponds to the realization of the RUL at time t_k . For simplicity, $t - t_k$ is defined as l_k . Theoretically, through a certain time scale transformation and failure threshold transformation, the RUL at time t_k is equal to the FPT of a new stochastic process $\{Z(l_k), l_k \geq 0\}$ crossing the failure threshold $w_k = w - x_k$, where $Z(l_k) = X(t_k + l_k) - x_k, Z(0) = 0$. Thus, taking the transformation $l_k = t - t_k, w_k = w - x_k$ with $l_k \geq 0$ for Equations (6), (7), (11), and (12), then the RUL of the degradation process $\{X(t), t \geq t_k\}$ could be obtained.

Let x_k and l_k denote the current degradation state and the RUL of the battery at time t_k , respectively. If the changing time τ is a known constant, using the observations up to t_k , the PDF of RUL based on the THDM considering unit-to-unit variability and the randomness of x_τ can be expressed as follows.

Case 1: The current time t_k is smaller than the changing time τ (i.e., $t_k < \tau$)

$$f_L(l_k) = \begin{cases} \frac{w - x_k}{\sqrt{2\pi l_k^2 (\sigma_{1r}^2 l_k^2 + \sigma_1^2 l_k)}} \\ \times \exp \left[-\frac{(w - x_k - \lambda_{1r} l_k)^2}{2(\sigma_{1r}^2 l_k^2 + \sigma_1^2 l_k)} \right], & 0 < t_k + l_k \leq \tau \\ S - T, & t_k + l_k > \tau \end{cases} \quad (13)$$

where $S = S_1 - S_2, T = T_1 - T_2$, and

$$\begin{aligned}
 S_1 &= \sqrt{\frac{r_{a2}^2}{2\pi(t_k + l_k - \tau)^2(\sigma_{\alpha 2}^2 + \sigma_{\beta 2}^2)}} \exp \left[-\frac{(\lambda_{\alpha 2} - \lambda_{\beta 2})^2}{2(\sigma_{\alpha 2}^2 + \sigma_{\beta 2}^2)} \right] \\
 &\times \left\{ \frac{\lambda_{\beta 2}\sigma_{\alpha 2}^2 + \lambda_{\alpha 2}\sigma_{\beta 2}^2}{\sigma_{\alpha 2}^2 + \sigma_{\beta 2}^2} \times \Phi \left(\frac{\lambda_{\beta 2}\sigma_{\alpha 2}^2 + \lambda_{\alpha 2}\sigma_{\beta 2}^2}{\sqrt{\sigma_{\alpha 2}^2\sigma_{\beta 2}^2(\sigma_{\alpha 2}^2 + \sigma_{\beta 2}^2)}} \right) \right\}
 \end{aligned}$$

$$\begin{aligned}
 &+ \left\{ \frac{\sigma_{\alpha 2}^2\sigma_{\beta 2}^2}{\sigma_{\alpha 2}^2 + \sigma_{\beta 2}^2} \times \phi \left(\frac{\lambda_{\beta 2}\sigma_{\alpha 2}^2 + \lambda_{\alpha 2}\sigma_{\beta 2}^2}{\sqrt{\sigma_{\alpha 2}^2\sigma_{\beta 2}^2(\sigma_{\alpha 2}^2 + \sigma_{\beta 2}^2)}} \right) \right\} \\
 S_2 &= \sqrt{\frac{r_{b2}^2}{2\pi(t_k + l_k - \tau)^2(\sigma_{\alpha 2}^2 + \sigma_{\beta 2}^2)}} \exp \left[-\frac{(\lambda_{\alpha 2} - \lambda_{\beta 2})^2}{2(\sigma_{\alpha 2}^2 + \sigma_{\beta 2}^2)} \right] \\
 &\times \left\{ 1 - \Phi \left(-\frac{\lambda_{\beta 2}\sigma_{\alpha 2}^2 + \lambda_{\alpha 2}\sigma_{\beta 2}^2}{\sqrt{\sigma_{\alpha 2}^2\sigma_{\beta 2}^2(\sigma_{\alpha 2}^2 + \sigma_{\beta 2}^2)}} \right) \right\} \\
 T_1 &= I_2 \times \sqrt{\frac{r_{a2}^2}{2\pi(t_k + l_k - \tau)^2(\sigma_{\alpha 2}^2 + \sigma_{\beta 2}^2)}} \\
 &\exp \left[-\frac{(\lambda_{\alpha 2} - \lambda_{\gamma 2})^2}{2(\sigma_{\alpha 2}^2 + \sigma_{\beta 2}^2)} \right] \\
 &\times \left\{ \frac{\lambda_{\gamma 2}\sigma_{\alpha 2}^2 + \lambda_{\alpha 2}\sigma_{\beta 2}^2}{\sigma_{\alpha 2}^2 + \sigma_{\beta 2}^2} \times \Phi \left(\frac{\lambda_{\gamma 2}\sigma_{\alpha 2}^2 + \lambda_{\alpha 2}\sigma_{\beta 2}^2}{\sqrt{\sigma_{\alpha 2}^2\sigma_{\beta 2}^2(\sigma_{\alpha 2}^2 + \sigma_{\beta 2}^2)}} \right) \right. \\
 &\left. + \sqrt{\frac{\sigma_{\alpha 2}^2\sigma_{\beta 2}^2}{\sigma_{\alpha 2}^2 + \sigma_{\beta 2}^2}} \times \phi \left(\frac{\lambda_{\gamma 2}\sigma_{\alpha 2}^2 + \lambda_{\alpha 2}\sigma_{\beta 2}^2}{\sqrt{\sigma_{\alpha 2}^2\sigma_{\beta 2}^2(\sigma_{\alpha 2}^2 + \sigma_{\beta 2}^2)}} \right) \right\} \\
 T_2 &= I_2 \times \sqrt{\frac{r_{b2}^2}{2\pi(t_k + l_k - \tau)^2(\sigma_{\alpha 2}^2 + \sigma_{\beta 2}^2)}} \\
 &\exp \left[-\frac{(\lambda_{\alpha 2} - \lambda_{\gamma 2})^2}{2(\sigma_{\alpha 2}^2 + \sigma_{\beta 2}^2)} \right] \\
 &\times \left\{ 1 - \Phi \left(-\frac{\lambda_{\gamma 2}\sigma_{\alpha 2}^2 + \lambda_{\alpha 2}\sigma_{\beta 2}^2}{\sqrt{\sigma_{\alpha 2}^2\sigma_{\beta 2}^2(\sigma_{\alpha 2}^2 + \sigma_{\beta 2}^2)}} \right) \right\} \\
 \lambda_{\alpha 2} &= \lambda_{2r} \int_{\tau}^{\tau+t_k} \mu(\rho - \tau; \vartheta) d\rho, \lambda_{\beta 2} = w - x_k - \lambda_{1r}(\tau - t_k), \\
 \lambda_{\gamma 2} &= -w + x_k - \lambda_{1r}(\tau - t_k) - \frac{2(w - x_k)\sigma_{1r}^2(\tau - t_k)}{\sigma_1^2}, \\
 \sigma_{\alpha 2}^2 &= \sigma_{2r}^2 \left(\int_{\tau}^{\tau+t_k+l_k} \mu(\rho - \tau; \vartheta) d\rho \right)^2 + \sigma_2^2(t_k + l_k - \tau), \\
 \sigma_{\beta 2}^2 &= (\tau - t_k)\sigma_1^2 + (\tau - t_k)^2\sigma_{1r}^2, \\
 r_{a2} &= \frac{(t_k + l_k - \tau)}{\sigma_{\alpha 2}^2} \\
 &\times \left(\sigma_2^2 + \sigma_{2r}^2 \mu(t_k + l_k - \tau; \vartheta) \int_{\tau}^{\tau+t_k+l_k} \mu(\rho - \tau; \vartheta) d\rho \right), \\
 r_{b2} &= \frac{(t_k + l_k - \tau)\sigma_2^2 (\lambda_{\alpha 2} - \lambda_{2r}(t_k + l_k - \tau) \mu(t_k + l_k - \tau; \vartheta))}{\sigma_{\alpha 2}^2}, \\
 I_2 &= \exp \left[\frac{2\lambda_{1r}(w - x_k)}{\sigma_1^2} \right] \\
 &+ \frac{2((w - x_k)^2\sigma_{1r}^4(\tau - t_k) + (w - x_k)^2\sigma_{1r}^2\sigma_1^2)}{(\sigma_1^2 + (\tau - t_k)\sigma_{1r}^2)\sigma_1^4} \quad (14)
 \end{aligned}$$

Case 2: The current time t_k is larger than the changing time τ (i.e., $t_k \geq \tau$)

$$f_L(l_k) \cong \frac{1}{\sqrt{2\pi l_k^2 \left[\sigma_{2r}^2 \left(\int_{t_k}^{t_k+l_k} \mu(\rho - \tau; \vartheta) d\rho \right)^2 + \sigma_2^2 l_k \right]^3}} \times \left[(w - x_k) \left(\sigma_{2r}^2 \left(\int_{t_k}^{t_k+l_k} \mu(\rho - \tau; \vartheta) d\rho \right)^2 + \sigma_2^2 l_k \right) - \left(\int_{t_k}^{t_k+l_k} \mu(\rho - \tau; \vartheta) d\rho - l_k \mu(t_k + l_k - \tau; \vartheta) \right) \times \left((w - x_k) \sigma_{2r}^2 \int_{t_k}^{t_k+l_k} \mu(\rho - \tau; \vartheta) d\rho + \lambda_{2r} \sigma_2^2 l_k \right) \right] \times \exp \left[\frac{(w - x_k - \lambda_{2r} \int_{t_k}^{t_k+l_k} \mu(\rho - \tau; \vartheta) d\rho)^2}{2 \left(\sigma_{2r}^2 \left(\int_{t_k}^{t_k+l_k} \mu(\rho - \tau; \vartheta) d\rho \right)^2 + \sigma_2^2 l_k \right)} \right] \quad (15)$$

It is worth mentioning that the changing time τ is a constant value in the above derivations of lifetime estimation and RUL prediction. In practice, due to the influence of operation switching and state transformation, different LIBs within the same batch have different changing times in their degradation paths. Therefore, it is more appropriate to define the changing time τ as a random variable to reflect such variability. In this case, based on the law of total probability, the distribution of lifetime and RUL could be derived as follows [36].

$$f_T(t) = \int_0^{+\infty} f_T(t|\tau) p(\tau) d\tau, f_L(l_k) = \int_{t_k}^{+\infty} f_L(l_k|\tau) p(\tau) d\tau \quad (16)$$

where $p(\tau)$ represents the PDF of the changing time τ . Since there is only one random variable in the above equation, it could be solved by some numerical methods, such as parabola approximation and trapezoidal approximation.

C. MODEL PARAMETER IDENTIFICATION

In this subsection, the unknown model parameters will be estimated based on historical observations and real-time monitoring data. The specific parameter identification process consists of changing point detection, offline parameter estimation, and online parameter updating.

1) OFFLINE CHANGING POINT DETECTION

It is assumed that the historical data of N LIBs from the same batch are known, i.e., $X = \{X_1, X_2, \dots, X_N\}$. The degradation data $X_n = \{x_{n,0}, x_{n,1}, \dots, x_{n,m_n}\}$ of the n -th battery is measured at time $\{t_{n,0}, t_{n,1}, \dots, t_{n,m_n}\}$, where m_n denotes the available number of measurements for the n -th battery. We further define that $\Delta x_{n,j} = x_{n,j} - x_{n,j-1}$ denotes the degradation increment of the n -th battery, where $j = 1, 2, \dots, m_n$. For simplicity, it is assumed that the sampling interval is fixed, i.e., $\Delta t = t_{n,j} - t_{n,j-1}$. In addition, let τ_n represents the

changing time of the n -th battery. To facilitate the computation, changing point location $\tilde{\tau}_n = \tau_n / \Delta t \in \{0, 1, \dots, m_n\}$ is assumed, videlicet, the changing point τ_n of each battery only appears at the measurement time $\{t_{n,0}, t_{n,1}, \dots, t_{n,m_n}\}$. Thus, $\{x_{n,0}, x_{n,1}, \dots, x_{n,\tilde{\tau}_n}\}$ is the observation in the first phase, whereas $\{x_{n,\tilde{\tau}_n+1}, x_{n,\tilde{\tau}_n+2}, \dots, x_{n,m_n}\}$ denotes the observation in the second phase. According to the property of the Wiener process, the degradation increment $\Delta x_{n,j}$ follows the normal distribution. Thus, the log-likelihood function of X_n can be formulated as follows,

$$\ln L(\lambda_{1,n}, \sigma_1, \lambda_{2,n}, \sigma_2, \vartheta, \tilde{\tau}_n | X_n) = \sum_{j=1}^{\tilde{\tau}_n} \ln \frac{1}{\sqrt{2\pi \sigma_1^2 \Delta t}} \exp \left[-\frac{(\Delta x_{n,j} - \lambda_{1,n} \Delta t)^2}{2\sigma_1^2 \Delta t} \right] + \sum_{j=\tilde{\tau}_n+1}^{m_n} \ln \frac{1}{\sqrt{2\pi \sigma_2^2 \Delta t}} \exp \left[-\frac{(\Delta x_{n,j} - \lambda_{2,n} \int_{t_{j-1}}^{t_j} \mu(\rho - \tau_n; \vartheta) d\rho)^2}{2\sigma_2^2 \Delta t} \right] \quad (17)$$

where $\lambda_{1,n}, \sigma_1, \lambda_{2,n}, \sigma_2, \vartheta$ and $\tilde{\tau}_n$ represent the parameters of THDM for the n -th battery.

For each battery, given the changing point location $\tilde{\tau}_n$, the maximum likelihood estimation (MLE) method is employed to obtain the drift and diffusion coefficients. However, due to the influence of the nonlinear drift function involved by the parameter ϑ , it is difficult to derive the estimated values of $\lambda_{1,n}, \sigma_1, \lambda_{2,n}, \sigma_2, \vartheta$, and $\tilde{\tau}_n$ by maximizing Equation (17). To solve this problem, inspired by [32], a profile log-likelihood function method with respect to ϑ is proposed as follows.

Firstly, if ϑ is known, the MLE values of $\lambda_{1,n}, \sigma_1, \lambda_{2,n}, \sigma_2, \vartheta$ can be calculated as,

$$\hat{\lambda}_{1,n} = \frac{\sum_{j=1}^{\tilde{\tau}_n} \Delta x_{n,j}}{\tilde{\tau}_n \Delta t}, \hat{\sigma}_{1,n} = \sqrt{\frac{1}{\tilde{\tau}_n} \sum_{j=1}^{\tilde{\tau}_n} \frac{(\Delta x_{n,j} - \hat{\lambda}_{1,n} \Delta t)^2}{\Delta t}} \quad (18)$$

$$\hat{\lambda}_{2,n}(\vartheta) = \frac{\sum_{j=\tilde{\tau}_n+1}^{m_n} \Delta x_{n,j} \int_{t_{j-1}}^{t_j} \mu(\rho - \tau_n; \vartheta) d\rho}{\sum_{j=\tilde{\tau}_n+1}^{m_n} \left(\int_{t_{j-1}}^{t_j} \mu(\rho - \tau_n; \vartheta) d\rho \right)^2},$$

$$\hat{\sigma}_{2,n}(\vartheta) = \sqrt{\frac{1}{m_n - \tilde{\tau}_n} \left[\sum_{j=\tilde{\tau}_n+1}^{m_n} \frac{(\Delta x_{n,j} - \hat{\lambda}_{2,n}(\vartheta) \int_{t_{j-1}}^{t_j} \mu(\rho - \tau_n; \vartheta) d\rho)^2}{\Delta t} \right]} \quad (19)$$

It is noted that $\hat{\lambda}_{1,n}$ and $\hat{\sigma}_{1,n}$ are independent of ϑ , which means that the results in Equation (18) are the optimal estimates. However, $\hat{\lambda}_{2,n}(\vartheta)$ and $\hat{\sigma}_{2,n}(\vartheta)$ in Equation (19) are functions of ϑ , thus, we need to solve ϑ first.

Secondly, since the two phases are independent of each other, by substituting Equation (19) into the second formula in Equation (17), the profile log-likelihood function of ϑ can be formulated as,

$$\begin{aligned} \ln L(\vartheta|X_n) &= \sum_{j=\tilde{\tau}_n+1}^{m_n} \ln \frac{1}{\sqrt{2\pi\hat{\sigma}_{2,n}^2(\vartheta)\Delta t}} \\ &\times \exp \left[-\frac{(\Delta x_{n,j} - \hat{\lambda}_{2,n}(\vartheta) \int_{t_{j-1}}^{t_j} \mu(\rho - \tau_n; \vartheta) d\rho)^2}{2\hat{\sigma}_{2,n}^2(\vartheta)\Delta t} \right] \end{aligned} \quad (20)$$

Thirdly, based on a search algorithm implemented by the “fminsearch” function in MATLAB, the estimate of ϑ , i.e., $\hat{\vartheta}$, can be calculated through maximizing the profile log-likelihood function in Equation (20). Finally, substituting $\hat{\vartheta}$ into Equation (19), the estimates of $\hat{\lambda}_{2,n}(\vartheta)$ and $\hat{\sigma}_{2,n}(\vartheta)$ could be obtained, respectively.

Then, substituting Equations (18) and (19) into Equation (17) gives the log-likelihood function $\ln L(\tilde{\tau}_n|X_n)$ that is only related to the changing point location $\tilde{\tau}_n$. By enumerating all possible values of $\tilde{\tau}_n$ in range $1 < \tilde{\tau}_n < m_n$ to maximize $\ln L(\tilde{\tau}_n|X_n)$, the optimal changing time $\hat{\tau}_n$ of the n -th battery can be obtained as follow,

$$\hat{\tau}_n = \Delta t \times \arg \max_{\tilde{\tau}_n} \ln L(\tilde{\tau}_n|\Delta X_n) \quad (21)$$

In addition, for the n -th battery that exhibits a two-phase hybrid deteriorating feature, assuming the current time is t_k . If $t_k > \hat{\tau}_n$, it indicates that the changing point has appeared and the changing time is a constant. On the contrary, $t_k < \hat{\tau}_n$ means that the changing point has not appeared. In this case, a common way is to define the changing time as a random variable and update its distribution.

It is assumed that the random changing time τ follows the normal distribution, i.e., $\tau \sim N(\mu_\tau, \sigma_\tau^2)$. Then, the estimated value $\hat{\tau}_n$ can be treated as the observations of τ . Therefore, the hyper-parameters of changing time can be obtained through statistical analysis,

$$\mu_\tau = \frac{1}{N} \sum_{n=1}^N \hat{\tau}_n, \sigma_\tau = \sqrt{\frac{1}{N} \sum_{n=1}^N (\hat{\tau}_n - \mu_\tau)^2} \quad (22)$$

2) OFFLINE PARAMETER ESTIMATION

When the changing time τ is obtained, according to Equation (1), the unknown parameters of THDM are $\{\lambda_1, \sigma_1, \lambda_2, \sigma_2, \vartheta\}$. Among them, $\sigma_1, \sigma_2, \vartheta$ are fixed parameters that describe the common degradation characteristics of LIBs from the same batch. $\lambda_1 \sim N(\lambda_{1r}, \sigma_{1r}^2)$ and $\lambda_2 \sim$

$N(\lambda_{2r}, \sigma_{2r}^2)$ are random variables that reflect the unit-to-unit variability. Therefore, the parameters that need to be estimated in THDM are defined as the parameter vector $\Theta = \{\lambda_{1r}, \sigma_{1r}, \sigma_1, \lambda_{2r}, \sigma_{2r}, \sigma_2, \vartheta\}$.

It is noted that the estimated values of $\{\hat{\lambda}_{1,1}, \hat{\lambda}_{1,2}, \dots, \hat{\lambda}_{1,n}\}$ and $\{\hat{\lambda}_{2,1}, \hat{\lambda}_{2,2}, \dots, \hat{\lambda}_{2,n}\}$ obtained in Section II-C-1) can be treated as the observations of the random variables λ_1 and λ_2 . Hence, λ_1 and λ_2 can be regarded as the latent variables driven by the hyper-parameters $\lambda_{1r}, \sigma_{1r}^2$ and $\lambda_{2r}, \sigma_{2r}^2$, respectively.

The expectation maximization (EM) algorithm is a stable and effective iterative approach, which has advantages in solving the hyper-parameter estimation problem involving hidden variables [55]. According to the EM algorithm, the complete log-likelihood function of the n -th battery can be formulated as follows,

$$\begin{aligned} \ln L(\Theta|X, Y) &= \ln p(X, Y|\Theta) \\ &= \ln \prod_{n=1}^N p(X_n, Y_n|\Theta) \\ &= \sum_{n=1}^N \ln (p(X_n|Y_n, \Theta)p(Y_n|\Theta)) \end{aligned} \quad (23)$$

where $Y_n = \{\lambda_{1,n}, \lambda_{2,n}\}$ denotes the latent variables of the n -th battery.

Let $\hat{\Theta}^{(k)} = \{\hat{\lambda}_{1r}^{(k)}, \hat{\sigma}_{1r}^{(k)}, \hat{\sigma}_1^{(k)}, \hat{\lambda}_{2r}^{(k)}, \hat{\sigma}_{2r}^{(k)}, \hat{\sigma}_2^{(k)}, \hat{\vartheta}^{(k)}\}$ represent the parameter estimates in the k -th step. Then, $\hat{\vartheta}^{(k+1)}$ could be calculated through the profile log-likelihood function method, which is similar to the approach proposed in Section II-C-1). Therefore, the next iteration $\hat{\Theta}^{(k+1)}$ could be obtained by calculating the conditional expectation $Q(\Theta|\hat{\Theta}^{(k)})$ in the E -step and computing $\hat{\Theta}^{(k+1)} = \arg \max_{\tilde{\tau}_n} Q(\Theta|\hat{\Theta}^{(k)})$ in the M -step based on the EM algorithm.

$$\begin{aligned} \hat{\lambda}_{1r}^{(k+1)} &= \frac{1}{N} \sum_{n=1}^N \varphi_1^{(k)} \\ \hat{\sigma}_{1r}^{(k+1)} &= \sqrt{\frac{1}{N} \sum_{n=1}^N \left[\varphi_1^{2,(k)} - 2\varphi_1^{(k)} \hat{\lambda}_{1r}^{(k+1)} + \left(\hat{\lambda}_{1r}^{(k+1)} \right)^2 \right]} \\ \hat{\sigma}_1^{(k+1)} &= \sqrt{\frac{\sum_{n=1}^N \left[\sum_{j=1}^{\tilde{\tau}_n} \Delta x_{n,j}^2 - 2\varphi_1^{(k)} \sum_{j=1}^{\tilde{\tau}_n} \Delta x_{n,j} \Delta t + \tilde{\tau}_n \varphi_1^{2,(k)} \Delta t^2 \right]}{\sum_{n=1}^N \tilde{\tau}_n \Delta t}} \end{aligned}$$

$$\begin{aligned}
& \hat{\lambda}_{2r}^{(k+1)} \\
&= \frac{1}{N} \sum_{n=1}^N \varphi_2^{(k)} \\
& \hat{\sigma}_{2r}^{(k+1)} \\
&= \sqrt{\frac{1}{N} \sum_{n=1}^N \left[\varphi_2^{2,(k)} - 2\varphi_2^{(k)} \hat{\lambda}_{2r}^{(k+1)} + \left(\hat{\lambda}_{2r}^{(k+1)} \right)^2 \right]} \\
& \hat{\sigma}_2^{(k+1)} \\
&= \sqrt{\frac{\sum_{n=1}^N \left[\sum_{j=\tilde{\tau}_n+1}^{m_n} \Delta x_{n,j}^2 - 2\varphi_2^{(k)} \sum_{j=\tilde{\tau}_n+1}^{m_n} \Delta x_{n,j} \eta(t_j) + \varphi_2^{2,(k)} \sum_{j=\tilde{\tau}_n+1}^{m_n} \eta^2(t_j) \right]}{\sum_{n=1}^N (m_n - \tilde{\tau}_n) \Delta t}}
\end{aligned} \quad (24)$$

where

$$\begin{aligned}
\varphi_1^{(k)} &= E[\lambda_{1,n} | X_n, \hat{\Theta}^{(k)}] \\
&= \frac{(x_n, \tilde{\tau}_n - x_n, 0) \Delta t \hat{\sigma}_{1r}^{2,(k)} + \hat{\sigma}_1^{2,(k)} \Delta t \hat{\lambda}_{1r}^{(k)}}{\tilde{\tau}_n \hat{\sigma}_{1r}^{2,(k)} \Delta t^2 + \hat{\sigma}_1^{2,(k)} \Delta t} \\
\varphi_1^{2,(k)} &= E[\lambda_{1,n}^2 | X_n, \hat{\Theta}^{(k)}] \\
&= \frac{\hat{\sigma}_{1r}^{2,(k)} \hat{\sigma}_1^{2,(k)} \Delta t}{\tilde{\tau}_n \hat{\sigma}_{1r}^{2,(k)} \Delta t^2 + \hat{\sigma}_1^{2,(k)} \Delta t} \\
&\quad + \left[\frac{(x_n, \tilde{\tau}_n - x_n, 0) \Delta t \hat{\sigma}_{1r}^{2,(k)} + \hat{\sigma}_1^{2,(k)} \Delta t \hat{\lambda}_{1r}^{(k)}}{\tilde{\tau}_n \hat{\sigma}_{1r}^{2,(k)} \Delta t^2 + \hat{\sigma}_1^{2,(k)} \Delta t} \right]^2 \\
\varphi_2^{(k)} &= E[\lambda_{2,n} | X_n, \hat{\Theta}^{(k)}] \\
&= \frac{\hat{\sigma}_{2r}^{2,(k)} \sum_{j=\tilde{\tau}_n+1}^{m_n} \Delta x_{n,j} \int_{t_{j-1}}^{t_j} \mu(\rho - \tau_n; \vartheta) d\rho + \hat{\sigma}_2^{2,(k)} \Delta t \hat{\lambda}_{2r}^{(k)}}{\hat{\sigma}_{2r}^{2,(k)} \sum_{j=\tilde{\tau}_n+1}^{m_n} \left(\int_{t_{j-1}}^{t_j} \mu(\rho - \tau_n; \vartheta) d\rho \right)^2 + \hat{\sigma}_2^{2,(k)} \Delta t} \\
\varphi_2^{2,(k)} &= E[\lambda_{2,n}^2 | X_n, \hat{\Theta}^{(k)}] \\
&= \frac{\hat{\sigma}_{2r}^{2,(k)} \hat{\sigma}_2^{2,(k)} \Delta t}{\hat{\sigma}_{2r}^{2,(k)} \sum_{j=\tilde{\tau}_n+1}^{m_n} \left(\int_{t_{j-1}}^{t_j} \mu(\rho - \tau_n; \vartheta) d\rho \right)^2 + \hat{\sigma}_2^{2,(k)} \Delta t} \\
&\quad + \left[\frac{\hat{\sigma}_{2r}^{2,(k)} \sum_{j=\tilde{\tau}_n+1}^{m_n} \Delta x_{n,j} \int_{t_{j-1}}^{t_j} \mu(\rho - \tau_n; \vartheta) d\rho + \hat{\sigma}_2^{2,(k)} \Delta t \hat{\lambda}_{2r}^{(k)}}{\hat{\sigma}_{2r}^{2,(k)} \sum_{j=\tilde{\tau}_n+1}^{m_n} \left(\int_{t_{j-1}}^{t_j} \mu(\rho - \tau_n; \vartheta) d\rho \right)^2 + \hat{\sigma}_2^{2,(k)} \Delta t} \right]^2 \\
\eta(t_j) &= \int_{t_{j-1}}^{t_j} \mu(\rho - \tau_n; \vartheta) d\rho \quad (25)
\end{aligned}$$

Proof: See Appendix C.

According to the convergence of the EM algorithm, the optimal parameter estimates can be obtained by iterating the

E -step and M -step until the convergence criterion $\|\hat{\Theta}^{(k+1)} - \hat{\Theta}^{(k)}\|$ is satisfied.

3) ONLINE PARAMETER UPDATING

For a certain operating battery, to reflect the individual degradation features, the hyper-parameters of λ_1 and λ_2 need to be updated online. If the current time is t_k , the degradation data corresponding to $\{t_0, t_1, \dots, t_k\}$ could be denoted as $X_{0:k} = \{x_0, x_1, \dots, x_k\}$. It is defined that the degradation increment is $\Delta x_j = x_j - x_{j-1}$, and the sampling interval is $\Delta t = t_j - t_{j-1}, j = 1, \dots, k$. Hence, $\Delta X_{1:k} = \{\Delta x_1, \Delta x_2, \dots, \Delta x_k\}$. Then, let $\lambda_{1r,0}, \sigma_{1r,0}$, and $\lambda_{2r,0}, \sigma_{2r,0}$ attained in Section II-C-2) represent the prior values of λ_1 and λ_2 , an online parameter updating procedure based on the Bayesian rule can be summarized as follows.

(1) When $t_k \leq \tau$, the changing point has not appeared, which means that only the drift coefficient λ_1 of the first phase needs to be updated, thus all observations $X_{0:k} = \{x_0, x_1, \dots, x_k\}$ could be utilized for updating. According to the Bayesian rule, the following results can be obtained,

$$p(\lambda_1 | X_{0:k}) \propto p(X_{0:k} | \lambda_1) p(\lambda_1) \quad (26)$$

where

$$\begin{aligned}
p(X_{0:k} | \lambda_1) &= \prod_{j=1}^k \frac{1}{\sqrt{2\pi\sigma_{1r}^2\Delta t}} \exp\left[-\frac{(\Delta x_j - \lambda_1 \Delta t)^2}{2\sigma_{1r}^2\Delta t}\right], \\
p(\lambda_1) &= \frac{1}{\sqrt{2\pi\sigma_{1r,0}^2}} \exp\left[-\frac{(\lambda_1 - \lambda_{1r,0})^2}{2\sigma_{1r,0}^2}\right] \quad (27)
\end{aligned}$$

It can be found that $p(X_{0:k} | \lambda_1)$ and $p(\lambda_1)$ follow the normal distribution. Thus, the posterior distribution $p(\lambda_1 | X_{0:k})$ could be obtained based on the properties of the conjugate normal distribution.

$$p(\lambda_1 | X_{0:k}) = \frac{1}{\sqrt{2\pi\sigma_{1r}^2}} \exp\left[-\frac{(\lambda_1 - \lambda_{1r})^2}{2\sigma_{1r}^2}\right] \quad (28)$$

with

$$\begin{aligned}
\lambda_{1r} &= \frac{\sigma_{1r,0}^2(x_k - x_0) + \sigma_{1r}^2\lambda_{1r,0}}{\sigma_{1r,0}^2(t_k - t_0) + \sigma_{1r}^2}, \\
\sigma_{1r} &= \sqrt{\frac{\sigma_{1r,0}^2\sigma_{1r}^2}{\sigma_{1r,0}^2(t_k - t_0) + \sigma_{1r}^2}} \quad (29)
\end{aligned}$$

(2) When $t_k > \tau$, i.e., the changing point has already appeared, the posterior distribution of λ_2 could be updated based on the observations $X_{\tilde{\tau}:k} = \{x_{\tilde{\tau}}, x_{\tilde{\tau}+1}, \dots, x_k\}$. Then we can have the following results,

$$\begin{aligned}
p(\lambda_2 | X_{\tilde{\tau}:k}) \\
\propto p(X_{\tilde{\tau}:k} | \lambda_2) p(\lambda_2) \quad (30)
\end{aligned}$$

$$\begin{aligned}
 & p(X_{\tilde{\tau}:k}|\lambda_2) \\
 &= \prod_{j=\tilde{\tau}+1}^k \frac{1}{\sqrt{2\pi\sigma_2^2\Delta t}} \exp\left[-\frac{(\Delta x_j - \lambda_2 \int_{t_{j-1}}^{t_j} \mu(\rho - \tau; \vartheta)d\rho)^2}{2\sigma_2^2\Delta t}\right], \\
 & p(\lambda_2) \\
 &= \frac{1}{\sqrt{2\pi\sigma_{2r,0}^2}} \exp\left[-\frac{(\lambda_2 - \lambda_{2r,0})^2}{2\sigma_{2r,0}^2}\right] \quad (31)
 \end{aligned}$$

Similar to the first phase, the posterior distribution $p(\lambda_2|X_{\tilde{\tau}:k})$ could be obtained as follows,

$$p(\lambda_2|X_{\tilde{\tau}:k}) = \frac{1}{\sqrt{2\pi\sigma_{2r}^2}} \exp\left[-\frac{(\lambda_2 - \lambda_{2r})^2}{2\sigma_{2r}^2}\right] \quad (32)$$

with

$$\begin{aligned}
 \lambda_{2r} &= \frac{\sigma_{2r,0}^2 \sum_{j=\tilde{\tau}+1}^k \Delta x_j \int_{t_{j-1}}^{t_j} \mu(\rho - \tau; \vartheta)d\rho + \sigma_2^2 \lambda_{2r,0} \Delta t}{\sigma_{2r,0}^2 \sum_{j=\tilde{\tau}+1}^k \left(\int_{t_{j-1}}^{t_j} \mu(\rho - \tau; \vartheta)d\rho\right)^2 + \sigma_2^2 \Delta t}, \\
 \sigma_{2r} &= \sqrt{\frac{\sigma_{2r,0}^2 \sigma_2^2 \Delta t}{\sigma_{2r,0}^2 \sum_{j=\tilde{\tau}+1}^k \left(\int_{t_{j-1}}^{t_j} \mu(\rho - \tau; \vartheta)d\rho\right)^2 + \sigma_2^2 \Delta t}} \quad (33)
 \end{aligned}$$

In this way, the estimates of λ_{1r} , σ_{1r} and λ_{2r} , σ_{2r} could be updated based on the Bayesian rule.

4) ONLINE CHANGING POINT DETECTION

Another important task in the online phase is to perform online changing point detection. For an operating battery, based on Lemma 2 in Appendix A, we could construct the log-likelihood function of the changing point as follows,

$$\begin{aligned}
 & \ln L(\hat{\tau}|\Delta X_{1:k}) \\
 &= \sum_{j=1}^{\tilde{\tau}} \ln \frac{1}{\sqrt{2\pi\sigma_1^2\Delta t}} \exp\left[-\frac{(\Delta x_j - \lambda_1 \Delta t)^2}{2\sigma_1^2\Delta t}\right] \\
 &+ \sum_{j=\tilde{\tau}+1}^k \ln \frac{1}{\sqrt{2\pi\sigma_2^2\Delta t}} \\
 &\exp\left[-\frac{(\Delta x_j - \lambda_2 \int_{t_{j-1}}^{t_j} \mu(\rho - \tau; \vartheta)d\rho)^2}{2\sigma_2^2\Delta t}\right] \\
 &= \sum_{j=1}^{\tilde{\tau}} \ln \int_{-\infty}^{+\infty} \frac{1}{\sqrt{2\pi\sigma_1^2\Delta t}} \exp\left[-\frac{(\Delta x_j - \lambda_1 \Delta t)^2}{2\sigma_1^2\Delta t}\right] \\
 &\times \frac{1}{\sqrt{2\pi\sigma_{1r}^2}} \exp\left[-\frac{(\lambda_1 - \lambda_{1r})^2}{2\sigma_{1r}^2}\right] d\lambda_1 \\
 &+ \sum_{j=\tilde{\tau}+1}^k \ln \int_{-\infty}^{+\infty} \frac{1}{\sqrt{2\pi\sigma_2^2\Delta t}}
 \end{aligned}$$

$$\begin{aligned}
 & \exp\left[-\frac{(\Delta x_j - \lambda_2 \int_{t_{j-1}}^{t_j} \mu(\rho - \tau; \vartheta)d\rho)^2}{2\sigma_2^2\Delta t}\right] \\
 &\times \frac{1}{\sqrt{2\pi\sigma_{2r}^2}} \exp\left[-\frac{(\lambda_2 - \lambda_{2r})^2}{2\sigma_{2r}^2}\right] d\lambda_2 \\
 &= \sum_{j=1}^{\tilde{\tau}} \ln \frac{1}{\sqrt{2\pi(\sigma_{1r}^2\Delta t^2 + \sigma_1^2\Delta t)}} \exp\left[-\frac{(\Delta x_j - \lambda_{1r}\Delta t)^2}{2(\sigma_{1r}^2\Delta t^2 + \sigma_1^2\Delta t)}\right] \\
 &+ \sum_{j=\tilde{\tau}+1}^k \ln \frac{1}{\sqrt{2\pi\left(\left(\int_{t_{j-1}}^{t_j} \mu(\rho - \tau; \vartheta)d\rho\right)^2 \sigma_{2r}^2 + \sigma_2^2\Delta t\right)}} \\
 &\times \exp\left[-\frac{(\Delta x_j - \lambda_{2r} \int_{t_{j-1}}^{t_j} \mu(\rho - \tau; \vartheta)d\rho)^2}{2\left(\left(\int_{t_{j-1}}^{t_j} \mu(\rho - \tau; \vartheta)d\rho\right)^2 \sigma_{2r}^2 + \sigma_2^2\Delta t\right)}\right] \quad (34)
 \end{aligned}$$

where σ_1 , σ_2 , ϑ are estimated offline through the method proposed in Section II-C-2), and λ_{1r} , σ_{1r}^2 , λ_{2r} , σ_{2r}^2 are updated online via the Bayesian rule presented in Section II-C-3). Then, the log-likelihood function $\ln L(\hat{\tau}|\Delta X_{1:k})$ in Equation (34) only has one unknown parameter τ . Similar to the offline changing point detection method in Section II-C-1), the optimal changing point $\hat{\tau}$ of the certain operating battery could be obtained by the enumeration approach. In addition, we need to determine whether the changing point has appeared at the current time t_k . As discussed in [36], if $\hat{\tau} = k\Delta t$, it means that the changing point does not appear, and if $\hat{\tau} < k\Delta t$, the changing time is at $\hat{\tau}$.

III. EXPERIMENTS

To verify the feasibility and effectiveness of the proposed method, numerical and practical experiments are conducted in this section. For better illustration, we compare the THDM proposed in this work with the two-phase linear degradation model considering the random degradation state at the changing point (Zhang's method) [36], the two-phase linear degradation model neglecting the randomness of the degradation state at the changing point (Liu's method) [47], and the traditional single-phase nonlinear degradation model (Si's method) [32]. The implementation details are as follows.

A. NUMERICAL SIMULATION PROCEDURE

In this subsection, a numerical simulation is implemented to verify the feasibility and effectiveness of the proposed method for parameter identification and RUL prediction. Without loss of generality, the following power function is used to denote the nonlinear term in THDM, i.e., $\int_{\tau}^t \mu(\rho - \tau; \vartheta)d\rho = (t - \tau)^a$, thus, $\mu(t - \tau; \vartheta) = a(t - \tau)^{a-1}$. This kind of power function has been widely used in degradation modeling practice [32]. Then, the THDM

defined in Equation (1) could be rewritten as follows,

$$X(t) = \begin{cases} x_0 + \lambda_1 t + \sigma_1 B(t), & 0 < t \leq \tau \\ x_\tau + \lambda_2(t - \tau)^a + \sigma_2 B(t - \tau), & t > \tau \end{cases} \quad (35)$$

where the parameter a replaces parameter ϑ .

Based on Equation (35), we adopt the Euler–Maruyama discretization policy [56], [57] to generate the simulated degradation data. In the following experiments, simulation degradation trajectories of different sample sizes could be generated based on the above-presented procedure, and then the verification of Monte Carlo simulation, changing point detection, offline parameter estimation, online parameter updating, and RUL prediction could be conducted, respectively.

First, to demonstrate the derivations of the lifetime estimation presented in this work, the Monte Carlo (MC) simulation is employed to compare with the analytical solutions of the lifetime. Here, we conduct the lifetime estimation with both random changing time and drift coefficients. In this case, the parameters are set as $\lambda_{1r} = 1.5$, $\sigma_{1r} = 0.3$, $\sigma_1 = 1$, $\lambda_{2r} = 1$, $\sigma_{2r} = 0.15$, $\sigma_2 = 3$, $a = 1.5$, $w = 500$, $\mu_\tau = 100$, and $\sigma_\tau = 1$. For better illustration, 100,000 sets of degradation trajectories are generated, and the discretization step size is $\Delta t = 0.1$. Then, the FPTs of these trajectories are collected and regarded as the realizations of their actual lifetime. It is noteworthy that the analytical results of the lifetime could be obtained based on combining the results of Equations (6), (11), (12), and (16) in Section II-B-2.

Second, to validate the feasibility of the offline parameter identification method proposed in this work, we generate different sizes of degradation trajectories with random changing time and drift coefficients using the aforementioned parameter settings. For each size of the degradation trajectories, the changing points are detected by the method proposed in Section II-C-1). Based on the estimates of the changing time, the distribution parameters of τ could be obtained through the statistical analysis method. Then, the EM algorithm in Section II-C-2) is utilized to conduct the offline parameter estimation.

In addition, five degradation trajectories are generated for the verification of the online changing point detection method proposed in Section II-C-4). It is noted that for a certain operating battery, the changing time and the drift coefficients are fixed values. Hence, the true parameters for the data generation of those paths are set and listed in Table 1. Then, the online changing point detections are conducted for those online paths.

Subsequently, Path1 in Table 1 is selected for RUL prediction. Then, based on the detected changing time and the prior information of the parameter estimation in the offline stage, the online parameter updating is implemented through the method proposed in Section II-C-3).

Finally, the PDFs of RUL at different sample points could be obtained according to whether the changing point

TABLE 1. True parameter settings of the degradation trajectories for online changing point detection.

Number	λ_1	σ_1	λ_2	σ_2	τ
Path1	1.271	1	1.071	3	101.1
Path2	1.613	1	0.778	3	99.1
Path3	1.518	1	0.813	3	100.0
Path4	1.110	1	1.176	3	100.3
Path5	1.376	1	0.820	3	98.5

appears. If the current time $t_k \leq \tau$, the changing point has not appeared, thus the RUL could be estimated by substituting the results of the offline parameter estimation, changing point detection, and online parameter updating into Equations (13), (14), and combining them with the conclusion of Equation (16) in Section II-B-2). In contrast, if $t_k > \tau$, the changing point has already appeared, the RUL could be directly estimated by Equation (15). For comparative purposes, we further obtain the mean RUL prediction results of Zhang’s method [36] and Si’s method [32]. To gain a fair comparison, we also utilize the same parameter identification method proposed in Section II-C. It is worth mentioning that in the parameter identification process (including changing point detection, offline parameter estimation, and online parameter updating) of Zhang’s method [36], by setting the nonlinear parameter a to 1, the second phase of our parameter identification process is changed to linear form to adapt to the two-phase linear degradation model. Besides, in Si’s method [32], the first phase of our parameter identification process (only consisting of offline parameter estimation and online parameter updating) is omitted to adapt to the single-phase nonlinear degradation model.

B. PRACTICAL CASE IMPLEMENTATION DETAILS

In this subsection, the practical degradation data set of LIBs obtained from the Massachusetts Institute of Technology and Stanford University [53] are utilized to illustrate our approach. Manufactured by A123 Systems (APR18650M1A), these battery cells have a nominal capacity of 1.1 Ah and a nominal voltage of 3.3 V. The battery dataset is divided into three batches (2017–05–12; 2017–06–30; 2018–04–12), each containing approximately 48 cells. For better illustration, the data of batch 2017–05–12 are adopted in our paper, which is widely used in RUL prediction studies [58], [59]. All batteries in this batch were cycled with one-step or two-step fast-charging policies (C1(Q1)–C2), and the charge-discharge cycle stopped after cycling to 80% of nominal capacity (0.88Ah). Additionally, the batteries were tested in the chamber at the same temperature of 30°C. In particular, five batteries in batch 2017–05–12 are selected and labeled as B01–B05, the details are listed in Table 2. In the method verification, the degradation data of B01–B04 are used for offline training, and B05 is adopted to update the model and predict the RUL.

TABLE 2. Charge protocol and cycle life details of the five battery cells.

Battery	Barcode	Cycle Life	Charge Policy
B01	EL150800460507	860	6C(50%)-3C
B02	EL150800460644	917	6C(50%)-3C
B03	EL150800463229	966	8C(15%)-3.6C
B04	EL150800460477	1014	12.6C(30%)-3.6C
B05	EL150800460647	1051	8C(15%)-3.6C

In most applications, LIBs reach the end of life (EOL) when the actual capacity is reduced to below 80% of the rated value [60], [61], [62]. Thus, given the actual capacity degradation processes of the A123 batteries, in this paper, the failure threshold is set as 80% of the rated capacity, i.e., 0.88 Ah. It is noticeable that the practical experiments are also composed of four major parts, namely changing point detection, offline parameter estimation, online parameter updating, and RUL prediction. The specific details are similar to the above-presented numerical simulation experiments, thus they are omitted here due to space limitations.

IV. RESULTS AND DISCUSSION

In this section, the experimental results of Section III are analyzed and discussed. We first present and analyze the results of the numerical experiments. It covers the presentation of model parameter identification, lifetime estimation, and RUL prediction. Subsequently, we discuss the practical experiment results and compare the effectiveness of the proposed method with other methods.

A. NUMERICAL SIMULATION RESULTS AND ANALYSIS

To verify the feasibility of life estimation, the comparison of the PDFs between MC simulation results and our analytical results is displayed in Fig. 2. It is clear from Fig. 2 that the deviations between the theoretical curve and the statistical histograms are small and acceptable, which means that the proposed method can achieve accurate lifetime estimation.

Based on the model parameters settings provided in Section III-A, Fig. 3 shows several typical simulated degradation paths with random changing time and drift coefficients, which are used to validate the effectiveness of the changing point detection and offline parameter estimation method proposed in this work. It is observable from Fig. 3 that those degradation paths exhibit two-phase hybrid deteriorating patterns consisting of a linear first phase and a nonlinear second phase. Besides, the actual changing point is marked in Fig. 3 for the following changing point detection bias evaluation.

The true values of the parameters and the estimated results with different sample sizes are shown in Table 2. It can be found that as the sample size increases, the results obtained by our method can gradually approach the true value. Moreover, it is noteworthy that compared to other parameters, the estimates of hyper-parameters σ_{1r} and σ_{2r} are affected heavily by the sample size.

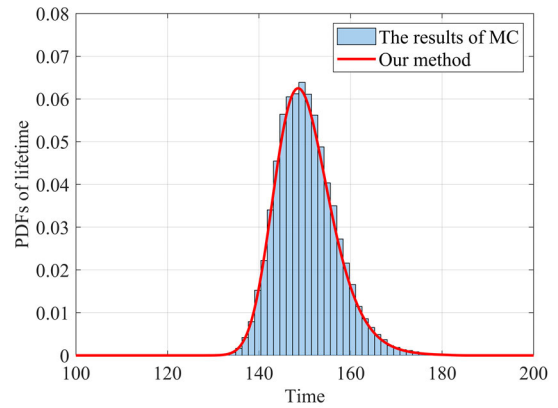


FIGURE 2. Comparison of analytical and simulation results for lifetime PDFs.

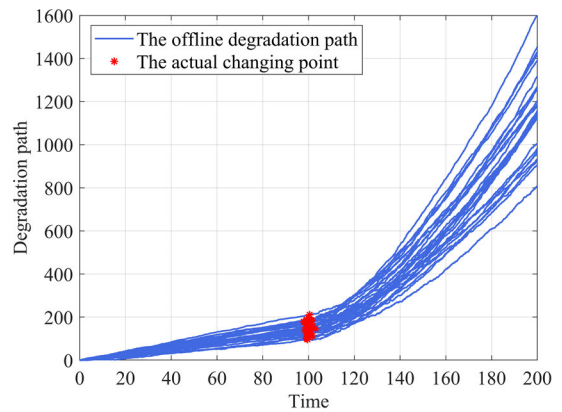


FIGURE 3. The simulated degradation trajectories.

To further demonstrate the superiority of the EM parameter estimation method proposed in Section II-C-2), the MLE method is used for comparison. We used the MLE method to estimate the parameter values for 1000 simulated degradation trajectories same as Table 2. The implementation details of the MLE method can be found in [36]. It is noteworthy that when constructing the log-likelihood function in the MLE method, we changed the second phase of the log-likelihood function to a nonlinear form to adapt to the nonlinear degradation trend in the second phase of the simulated degradation trajectories. Besides, since the estimates of the changing point distribution parameters μ_τ and σ_τ in Table 2 were originally based on the MLE method in Equation (22). Hence, the estimated values of μ_τ and σ_τ are not compared here. The estimation results of each parameter based on the MLE method are $\lambda_{1r} = 1.493$, $\sigma_{1r} = 0.312$, $\sigma_1 = 0.998$, $\lambda_{2r} = 1.072$, $\sigma_{2r} = 0.164$, $\sigma_2 = 3.002$, and $a = 1.479$. By comparing these results and the estimated parameters under the sample size 1000 with the true values in Table 3, it can be found that compared to the MLE method, the parameter estimates of the EM algorithm proposed in this paper are mostly closer to the true values, which indicates that the proposed EM algorithm has higher estimation accuracy than the MLE algorithm.

TABLE 3. Parameter estimation results with different sample sizes.

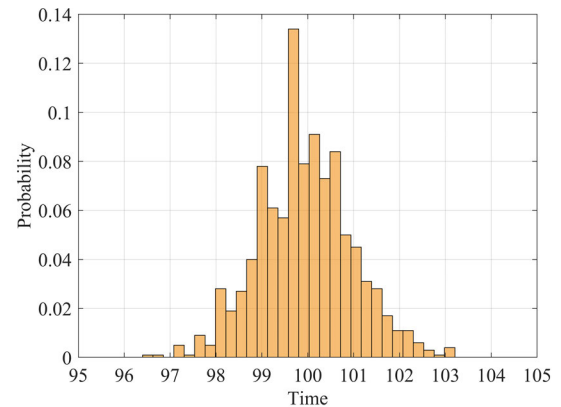
Size	5	50	100	500	1000	True Value
λ_{1r}	1.532	1.526	1.516	1.505	1.495	1.5
σ_{1r}	0.214	0.308	0.288	0.293	0.295	0.3
σ_1	0.996	0.997	1.000	1.000	0.999	1
λ_{2r}	0.788	0.926	0.928	0.961	0.942	1
σ_{2r}	0.088	0.125	0.138	0.143	0.142	0.15
σ_2	2.976	2.989	2.992	3.004	3.006	3
a	1.562	1.520	1.515	1.511	1.512	1.5
μ_τ	100.200	100.148	100.003	99.954	99.951	100
σ_τ	1.112	1.074	1.086	1.018	1.017	1

In addition, the histogram of the changing time detection results under the 1000 sample size is shown in Fig. 4(a). It can be seen from Fig. 4(a) that the estimated changing points are concentrated around $t = 100$, which are very close to the true value of μ_τ . Furthermore, the deviations of the true changing time and their estimates for 1000 trajectories are counted, and the results are shown in Fig. 4(b). It can be found that the bias is acceptable.

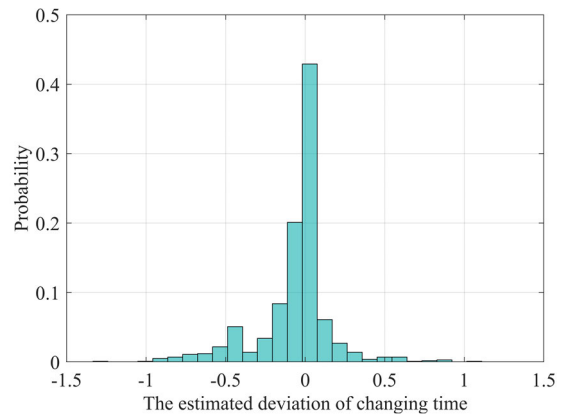
Following Fig. 5 shows the five online degradation trajectories (i.e., Path1-Path5 generated based on the preset parameters of Table 1 in Section III-A) for changing point detection and the corresponding log-likelihood variation trends. For those online paths, once the new observation data is available, the log-likelihood $\ln L(\hat{\tau}|\Delta X_{1:k})$ with respect to the changing point τ is calculated based on the online changing time detection method proposed in Section II-C-4). It is noted that the time corresponding to the maximum log-likelihood value is the optimal changing point.

The changing point detection results of these five online paths are listed in Table 4. In addition, to quantitatively evaluate the performance of the proposed online changing point detection method, the relative error (RE) is utilized to characterize the error between the detected changing point and the true value, as shown in Table 4. It can be found from Table 4 that the REs of the detected changing points are smaller than 1%, which indicates the effectiveness of the proposed online changing point detection method.

To improve the accuracy of RUL prediction, the results of $n = 1000$ size in Table 3 are treated as the prior information of λ_1 and λ_2 . Besides, the changing point detected result of Path1 in Table 4 is used for online parameter updating and RUL prediction. As shown in Fig. 6, when newly observed data are coming, the estimates of the hyper-parameters can be updated through the method in Section II-C-3). Despite the deviations between the prior parameter estimates and the true values of this online path, the parameter updating curves could gradually approach the actual values. In addition, it is observable that σ_{1r} and σ_{2r} are gradually decreasing as the observations accumulate, indicating that the uncertainty of estimation is reduced. It is worth noting that the unit is



(a) The estimated changing time.

(b) Deviations between τ_n and its estimates.**FIGURE 4.** The offline changing point detection results for 1000 degradation trajectories.**TABLE 4.** The online changing point detection results.

Number	Path1	Path2	Path3	Path4	Path5
True τ	101.1	99.1	100.0	100.3	98.5
Detected τ	100.8	99.2	100.7	100.4	98.7
RE	0.297%	0.101%	0.700%	0.100%	0.203%

omitted in Figs. 2-6 as the degradation paths are generated through simulation.

Since the preset failure threshold w is 500, it can be seen from Fig. 5(a) that the actual lifetime of the online degradation trajectory (Path1) is $T = 150$ according to the concept of FPT. Then, based on the updating results of the parameter estimates, the PDFs of RUL at different sample points are obtained and shown in Fig. 7(a). It can be seen from Fig. 7(a) that the estimated RULs and the actual values almost coincide, indicating that our method can effectively predict the RUL of the two-phase hybrid deteriorating LIBs. For better illustration, the mean RUL prediction results obtained from our work are compared with the results of Zhang's method [36], Liu's method [47], and Si's method [32], as shown in Fig. 7(b). It can be found that the mean RUL prediction results of our method are more accurate than the other three methods.

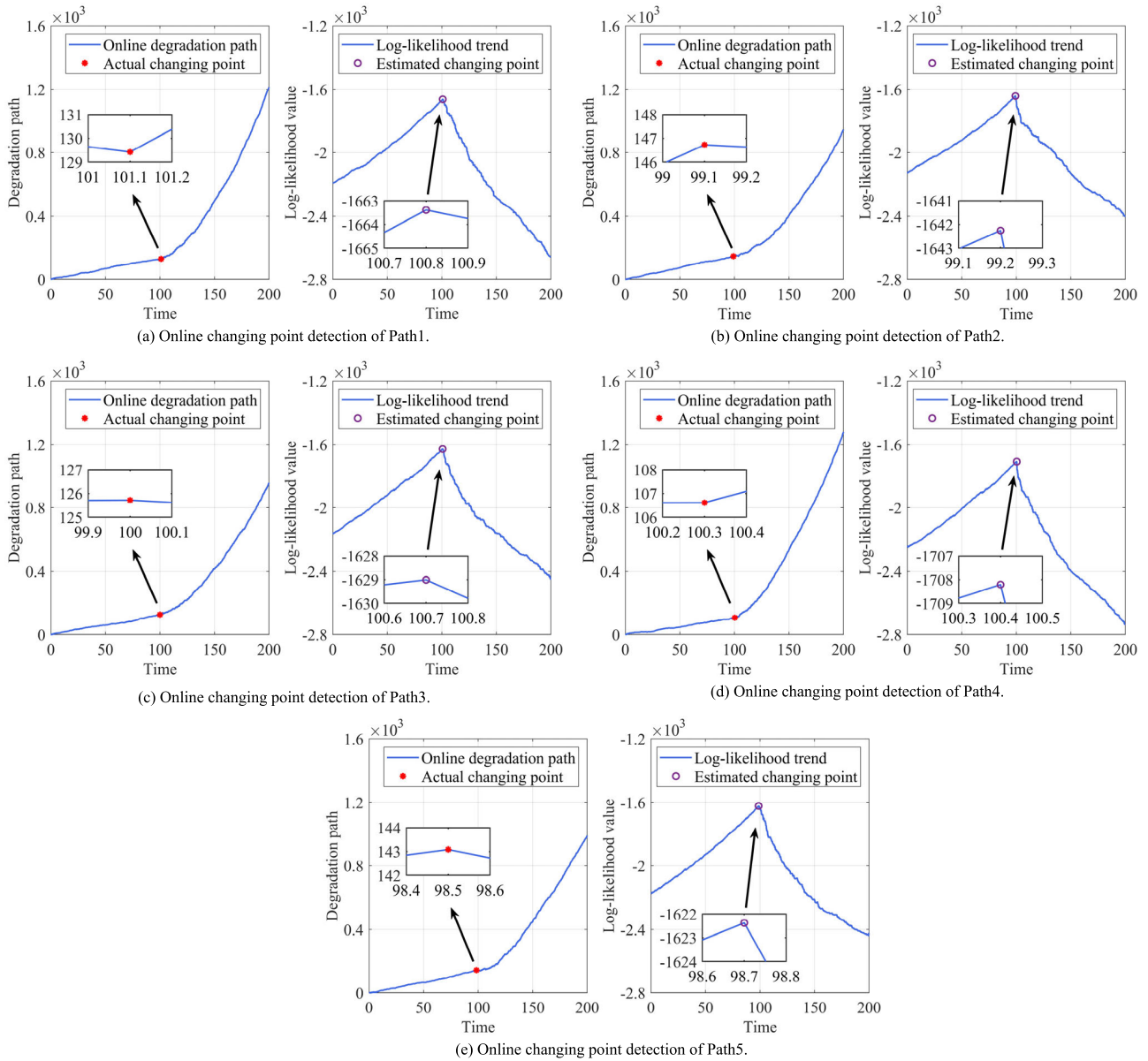


FIGURE 5. The online degradation trajectories and changing point detection process.

Furthermore, the mean RUL curve of Zhang’s method [36] is relatively stable during the first phase, however, it has a large estimation bias in the second phase. That is mainly because the online degradation path exhibits a two-phase hybrid deteriorating pattern, especially since the second phase has nonlinear characteristics, which may not be well fitted by the two-phase linear model established by Zhang’s method [36]. Besides, the mean RUL curve of Liu’s method [47] has a large bias in both phases, and there is a significant change near the changing point. That is because the degradation model of Liu’s method [47] is a two-phase linear degradation model without considering the randomness of the degradation state at the changing point as well as the nonlinearity of the second phase. In addition, It can be seen

from Fig. 7(b) that the deviations between the estimated mean RUL and the actual values of Si’s method [32] are large in the first phase but the biases decrease in the second phase. The reason is that Si’s method [32] is a single-phase model and does not consider the impact of the changing point. Therefore, it leads to significant RUL estimation bias throughout the first phase. However, after the changing point appears, the online degradation path is equivalent to a single-phase nonlinear degradation process. Thus, Si’s method [32] could effectively fit the degradation path in the second phase.

Overall, the simulation study demonstrates that the proposed method can achieve accurate RUL prediction, which could illustrate the feasibility and effectiveness of our approach in theory.

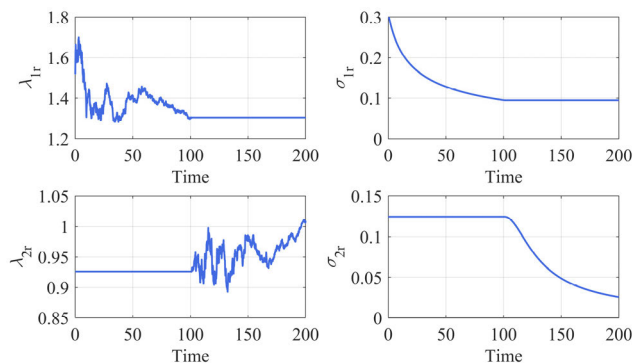


FIGURE 6. The updating of parameter estimates for a certain online degradation process.

B. PRACTICAL CASE RESULTS AND ANALYSIS

For the results of the practical experiments, Fig. 1 presents the capacity degradation trajectories of the five batteries mentioned in Section III-B. It can be seen from Fig. 1 that the degradation paths exhibit two-phase hybrid deteriorating characteristics. Furthermore, the LIBs of the same specification show significant heterogeneity in cycle life, which may be caused by different charging protocols. Based on the parameter identification method proposed in Section II-C, the detected changing times of Battery B01-B04 are 418, 435, 468, and 570 cycle, respectively. Besides, the parameter estimation results and the distribution parameters of the changing time are listed in Table 3. It can be found that the estimated values of the drift coefficients' hyper-parameters are relatively small. The reason is that the LIBs capacity only decreased by approximately 0.2 Ah after about 1000 cycles, thus, the degradation trajectories are flat and the degradation rates are low. Furthermore, it is worth noting that the hyper-parameters of λ_2 in the second phase are much smaller than the hyper-parameters of λ_1 in the first phase due to the influence of the nonlinear term parameter a . In addition, the parameter estimation results of Zhang's method [36] and Si's method [32] are summarized in Table 3. It is noted that we adopt the EM algorithm developed in Section II-C-2) to estimate the unknown model parameters of Zhang's method [36] and Si's method [32] to keep a fair comparison. Then, to compare the fitness of the three models, the Akaike information criterion (AIC) is applied [30].

$$AIC = 2(p - \max L) \quad (36)$$

where p denotes the number of estimated model parameters, and $\max L$ is the maximized likelihood function value.

Since the AIC considers both the number of model parameters and the log-likelihood, it can be adopted to select the best fitness model in engineering practice. Thus, the model complexity and fitting accuracy could achieve a balance. It is noticeable that the smallest value of AIC corresponds to the most suitable model.

The results of the model selection, i.e., AIC are detailed in Table 5. It is clear from Table 5 that our model has the

smallest AIC among the four models, which demonstrates that the two-phase hybrid degradation model with a linear first phase and a nonlinear second phase is most appropriate to fit the data of the LIBs.

Next, the data of battery B05 is selected to illustrate the RUL prediction process. Based on the online changing point detection method proposed in Section II-C-4), the log-likelihood $\ln L(\hat{\tau}|\Delta X_{1:k})$ is updated when new degradation data becomes available, and the log-likelihood variation trend is presented in Fig. 8. It can be observed from Fig. 8 that the detected changing time of battery B05 is 623 cycle.

Then, the online parameter updating could be realized through the method in Section II-C-3), as shown in Fig. 9. It can be found from Fig. 9 that the values of σ_{1r} and σ_{2r} are gradually decreasing, indicating that as the cycles of the battery accumulate, the uncertainty of parameter estimation decreases.

After updating the parameters' estimates based on the Bayesian rule, the estimated PDFs of RUL at different sample points are obtained as shown in Fig. 10(a). In addition, we further obtained the estimated RUL of Zhang's method [36] Liu's method [47], and Si's method [32] as shown in Fig. 10(b)-(d), respectively. It can be seen from Fig. 10 that the RUL PDFs of our method are closely distributed around the actual RUL values, indicating that our method can effectively conduct the RUL prediction of the battery degradation data.

It is noticeable that in Fig. 10, the red dashed lines represent the mean RUL estimation results, and the black dashed lines denote the actual RUL. It can be observed from Fig. 10 that although the estimated RULs of our method, Liu's method [47], and Si's method [32] have deviations in the early phase, the accuracy of RUL prediction gradually improves as the number of cycles increases in the following phase. Because the biased prior information has a significant impact on the accuracy of RUL prediction in the early phase. Fortunately, as the available observation data increase, the model parameters are updated in real-time, thus, the RUL prediction bias decreases in the following phase.

Besides, it is clear from Fig. 10 that the deviations between the mean RUL estimates of Zhang's method [36] and the actual RUL values are large in the second phase. This is mainly because the degradation trajectory of battery B05 exhibits two-phase hybrid deteriorating features, especially, the second phase has nonlinear characteristics. As a two-phase linear model, Zhang's method [36] is inadequate to characterize the nonlinearity of the second phase effectively. In addition, influenced by the random degradation state at the changing point, the RUL estimation bias of Liu's method [47] and Si's method [32] is relatively large in the first phase. However, the RUL estimation bias of Si's method [32] decreases faster than Liu's method [47] in the second phase owing to the ability of Si's method [32] to capture the nonlinear degradation characteristics. From the overall RUL

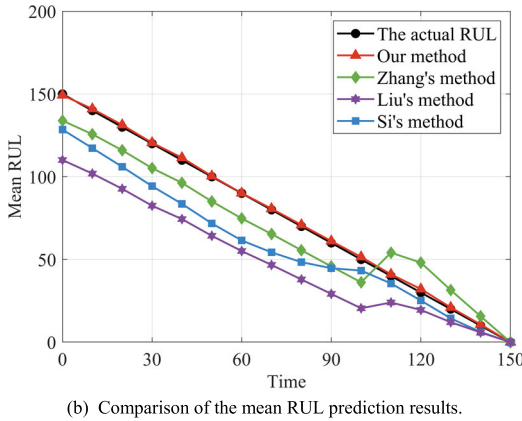
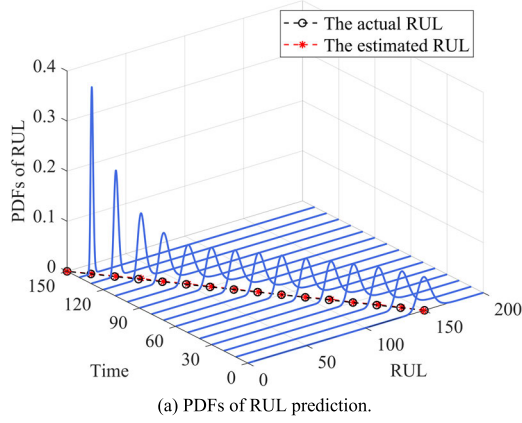


FIGURE 7. RUL prediction results for the online degradation path.

prediction results in Fig. 10, It can be found that our method has a higher accuracy in RUL prediction compared to the other three methods.

For better illustration, the quantitative evaluation metrics of mean squared error (MSE) [63], absolute error (AE), and RE are utilized to evaluate the RUL prediction performance of the three models. The MSE at each monitoring time point could be denoted as follows,

$$MSE_k = \int_0^{+\infty} (\tilde{l}_k - l_k)^2 f_L(l_k) dl_k \quad (37)$$

where \tilde{l}_k denotes the actual RUL at t_k , and $f_L(l_k)$ is the corresponding PDF of the RUL.

The AE between the predicted RUL and the actual RUL values at each monitoring time point could be defined as,

$$AE_k = \tilde{l}_k - \hat{l}_k \quad (38)$$

where \hat{l}_k denotes the estimated RUL at t_k .

The RE of the estimated RUL and the actual values at t_k could be represented as,

$$RE_k = \frac{|\tilde{l}_k - \hat{l}_k|}{\tilde{l}_k} \quad (39)$$

It is worth noting that the smallest value of the above metrics corresponds to the best RUL prediction result.

TABLE 5. The parameter estimation results of battery B01-B04.

Variable	Our method	Zhang's method	Liu's method	Si's method
λ_{1r}	-3.522e-5	-3.692e-5	-3.548e-5	-
σ_{1r}	6.876e-6	5.125e-6	9.751e-6	-
σ_1	2.489e-4	2.448e-4	2.230e-4	-
λ_{2r}	-1.519e-8	-4.076e-4	-3.923e-4	-1.245e-9
σ_{2r}	1.675e-9	6.776e-5	-3.656e-5	1.382e-10
σ_2	4.145e-4	4.926e-4	4.721e-4	3.096e-4
a	2.647	-	-	2.816
μ_τ	472.750	460.750	475.25	-
σ_τ	58.955	31.721	40.351	-
AIC	-1.249e4	-1.127e4	-1.021e4	-1.059e4

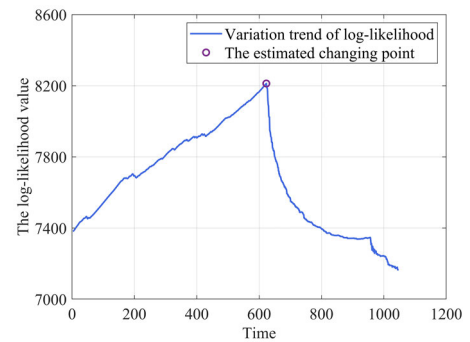


FIGURE 8. The log-likelihood variation trend of battery B05.

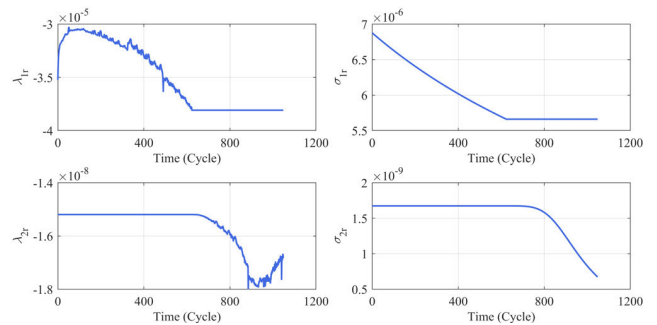


FIGURE 9. The online parameter updating process for battery B05.

Subsequently, we calculated the values of MSE, AE, and RE of the estimated RUL, as presented in Fig. 11. It can be found from Fig. 11(a) that compared to Zhang's method [36], Liu's method [47], and Si's method [32], the MSE values of our method maintain a relatively low level. Then, it is observable from Fig. 11(b) and (c) that the AE and the RE values of the proposed method are smaller than the other three methods. The quantitative results of these three criteria indicate that our method has higher prediction accuracy. Besides, it can be found from Fig. 11 that the MSE, AE, and RE values of Liu's method [47] and Si's method [32] are larger than our method and Zhang's method [36] in the first phase. That is mainly because the degradation models constructed by Liu's method [47] and Si's method [32] did not consider

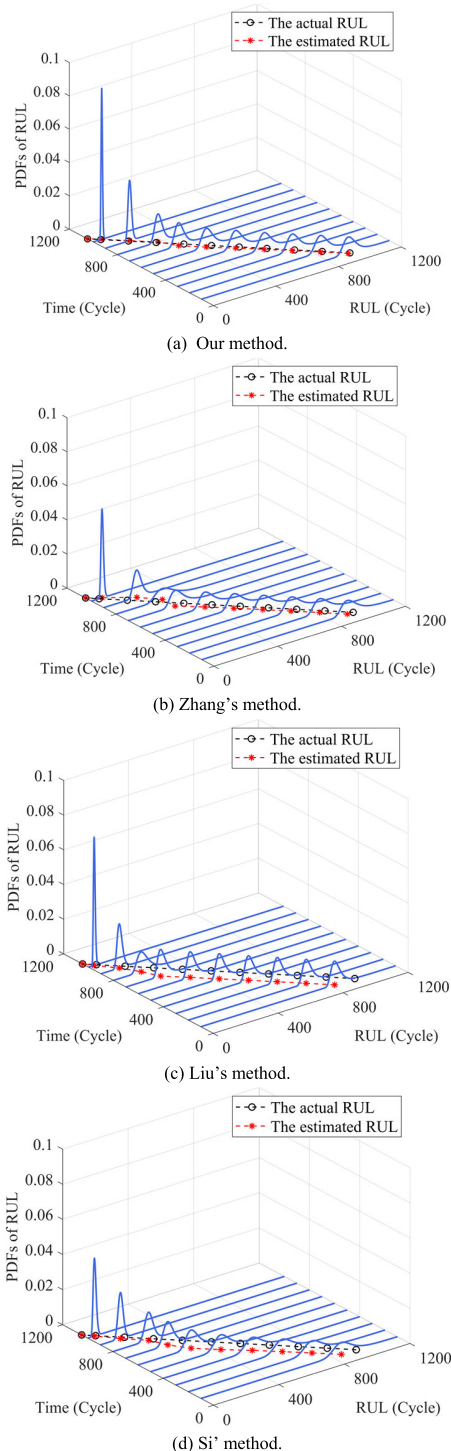


FIGURE 10. PDFs of RUL prediction for battery B05.

the influence of the random degradation state at the changing point, which lead to significant RUL estimation biases in the first phase. In addition, after the changing point appears, the nonlinear model of our method and Si's method [32] could characterize the nonlinear features of the second phase well, thus, the MSE values are smaller than Zhang's method [36] and Liu's method [47].

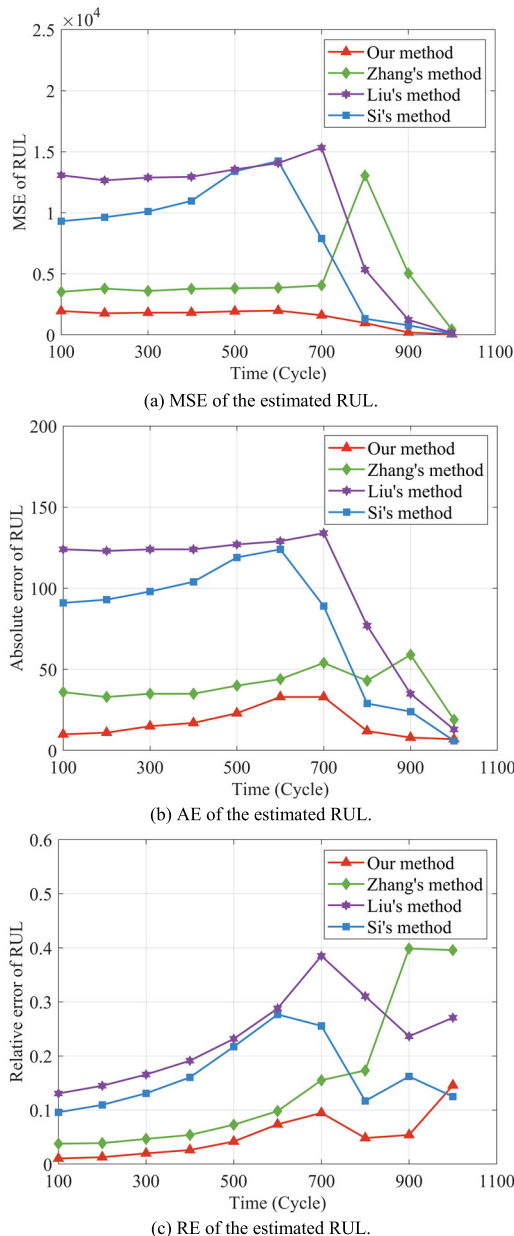


FIGURE 11. Performance evaluation of RUL prediction based on battery B05 degradation data.

In addition, It is observable from Fig. 11 that Zhang's method [36] has a large MSE value at the 800-th cycle in the second phase, which is much greater than the results of the other three methods. To investigate the reasons for this phenomenon, we further present the PDFs of the estimated RUL at the 800-th cycle, as shown in Fig. 12. According to the definition of MSE in Equation (37), a flat PDF curve means that the variance of the RUL estimate is large. Meanwhile, the large deviations between the mean RUL prediction results and the actual values, combined with the large variance, will result in a large MSE value. It can be observed from Fig. 12 that the deviation between the estimated RUL of Zhang's method [36] and the true value is relatively far compared to the other three

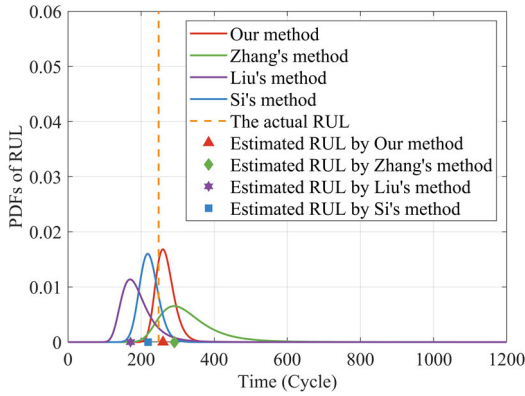


FIGURE 12. Comparison of RUL PDFs at the 800-th cycle.

methods, besides, its PDF curve is flatter than the other three methods, which leads to its maximum MSE value at the 800-th cycle. In contrast, it can be found that the estimated PDF of our method can cover the actual RUL well. Furthermore, even though the steepness of our PDF curve is similar to that of Si's method [32], the mean RUL prediction result of our method is closer to the actual RUL value compared to the other three methods, which demonstrates the superiority of our approach.

To further compare the RUL prediction performance of the proposed approach with the existing methods quantitatively, three metrics are employed as evaluation indicators, including the total mean-squared error (TMSE) [32], the mean absolute error (MAE) [64], and the cumulative relative accuracy (CRA) [65].

The TMSE is defined as the sum of the MSE at each observation point over the whole life cycle, which can be represented as,

$$TMSE = \sum_{k=1}^m MSE_k \quad (40)$$

where m denotes the number of observations.

The MAE characterizes the average absolute deviations between the estimated result and the true value. Based on the AE_k defined in Equation (38), the MAE can be formulated as,

$$MAE = \frac{1}{m} \sum_{k=1}^m AE_k \quad (41)$$

The third metric CRA is adopted to evaluate the relative prediction accuracy of the RUL over time, which could be defined as,

$$CRA = \frac{1}{m} \sum_{k=1}^m \left(1 - \frac{AE_k}{\tilde{l}_k} \right) \quad (42)$$

where \tilde{l}_k is defined in Equation (37).

It is worth noting that smaller TMSE and MAE values indicate higher accuracy in RUL prediction. By contrast, a higher CRA value that is close to 1 means the RUL estimation method is more accurate.

TABLE 6. Comparison results of RUL estimation based on TMSE, MAE, and CRA.

Metric	TMSE	MAE	CRA
Our method	1.385e6	16.183	0.951
Zhang's method [36]	4.572e6	43.121	0.847
Liu's method [47]	9.126e6	103.854	0.769
Si's method [32]	7.978e6	77.962	0.833

The quantitative comparison results of the estimated RUL according to the aforementioned metrics are detailed in Table 6. It is observable from Table 6 that our method yields lower TMSE and MAE values compared with the other three methods. As to the CRA metric, our method has the highest CRA value among the four methods, which indicates that our method can achieve more accurate RUL estimation results.

In summary, the practical experiments indicate that our method is effective and applicable for the hybrid deteriorating LIBs.

V. CONCLUSION

This paper investigates the degradation modeling and RUL prediction issues for the two-phase hybrid deteriorating LIBs with a linear first phase and a nonlinear second phase. To this end, a two-phase hybrid degradation model based on the Wiener process is presented to characterize the considered deteriorating patterns. Then, the analytical forms of the lifetime and RUL distribution are derived according to the FPT concept. Specifically, to fully consider the random effects caused by the unit heterogeneity, the drift parameters, changing time, and corresponding degradation state at the changing point are assumed to be random variables in the degradation model. In addition, the EM algorithm and the Bayesian rule are utilized to conduct the parameter identification jointly. For detail, incorporating the historical observations of the analogous LIBs, the EM algorithm in conjunction with a profile log-likelihood function method is adopted for offline parameter estimation. Subsequently, once the new observation becomes available, the online parameter updating is realized by the Bayesian rule for a certain operating battery. Finally, the effectiveness of our approach is validated based on the experiments of a numerical simulation and a practical case study of LIBs. The quantitative comparison results of the metrics MSE, AE, RE, and TMSE, etc. demonstrate that the proposed two-phase hybrid degradation model-based RUL prediction method is more accurate than the two-phase linear degradation model and traditional single-phase nonlinear degradation model, thus, opens a new avenue for the degradation modeling and RUL prediction of the two-phase hybrid deteriorating LIBs.

Although the proposed method can provide accurate RUL prediction for the two-phase hybrid deteriorating LIBs, there are several directions worth further investigating in the future.

First, in this work, only the two-phase hybrid degradation model is considered. However, in practice, due to the

complex changes in internal degradation mechanisms, the degradation processes of some LIBs may exhibit two-phase nonlinear characteristics or multi-phase features with linear and nonlinear degradation phases. Hence, the RUL prediction of such LIBs needs to be further explored. Second, this paper mainly focuses on the case that the observations are perfect measurements for degradation. However, the monitoring data of batteries usually have measurement errors in practice. Therefore, the hybrid degradation modeling and RUL prediction method considering the measurement variability will be challenging but practical research.

APPENDIX A

PROOF OF EQUATIONS (6),(7)

To calculate the PDF of the lifetime T , Lemma 2 [30] is introduced.

Lemma 2: If $Z \sim N(\lambda_b, \sigma_b^2)$, $\xi, U, V \in R$, and $W \in R^+$, then the following forms are formulated,

$$E_Z \left[\exp \left(-\frac{(\xi - VZ)^2}{2W} \right) \right] = \sqrt{\frac{W}{V^2\sigma_b^2 + W}} \exp \left(-\frac{(\xi - V\lambda_b)^2}{2(V^2\sigma_b^2 + W)} \right) \quad (43)$$

$$E_Z \left[(\xi - UZ) \exp \left(-\frac{(\xi - VZ)^2}{2W} \right) \right] = \sqrt{\frac{W}{V^2\sigma_b^2 + W}} \left(\xi - U \frac{V\sigma^2\xi + \lambda_b W}{V\sigma_b^2 + W} \right) \exp \left(-\frac{(\xi - V\lambda_b)^2}{2(V^2\sigma_b^2 + W)} \right) \quad (44)$$

Based on Lemma 2, the PDF of the lifetime T for THDM with unit-to-unit variability could be obtained.

(1) if $0 < t \leq \tau$,

$$\begin{aligned} f_T(t) &= \int_{-\infty}^{+\infty} f_T(t|\lambda_1)p(\lambda_1)d\lambda_1 \\ &= \int_{-\infty}^{+\infty} \frac{w-x_0}{\sqrt{2\pi\sigma_1^2 t^3}} \exp \left[-\frac{(w-x_0-\lambda_1 t)^2}{2\sigma_1^2 t} \right] \\ &\quad \times \frac{1}{\sqrt{2\pi\sigma_{1r}^2}} \exp \left[-\frac{(\lambda_1-\lambda_{1r})^2}{2\sigma_{1r}^2} \right] d\lambda_1 \\ &= E_{\lambda_1} \left[\frac{w-x_0}{\sqrt{2\pi\sigma_1^2 t^3}} \exp \left[-\frac{(w-x_0-\lambda_1 t)^2}{2\sigma_1^2 t} \right] \right] \\ &= \frac{w-x_0}{\sqrt{2\pi t^2(\sigma_{1r}^2 t^2 + \sigma_1^2 t)}} \exp \left[-\frac{(w-x_0-\lambda_{1r} t)^2}{2(\sigma_{1r}^2 t^2 + \sigma_1^2 t)} \right] \end{aligned} \quad (45)$$

(2) if $t > \tau$,

$$f_T(t|x_\tau)$$

$$\begin{aligned} &= \int_{-\infty}^{+\infty} f_T(t|\lambda_2, x_\tau)p(\lambda_2)d\lambda_2 \\ &\cong \int_{-\infty}^{+\infty} \frac{w-x_\tau-\lambda_2 \left(\int_\tau^t \mu(\rho-\tau; \vartheta)d\rho - (t-\tau)\mu(t-\tau; \vartheta) \right)}{\sigma_2 \sqrt{2\pi(t-\tau)^3}} \\ &\quad \times \exp \left[-\frac{\left(w-x_\tau-\lambda_2 \int_\tau^t \mu(\rho-\tau; \vartheta)d\rho \right)^2}{2\sigma_2^2(t-\tau)} \right] \\ &\quad \times \frac{1}{\sqrt{2\pi\sigma_{2r}^2}} \exp \left[-\frac{(\lambda_2-\lambda_{2r})^2}{2\sigma_{2r}^2} \right] d\lambda_2 \\ &\cong \frac{1}{\sqrt{2\pi(t-\tau)^2 \left[\sigma_{2r}^2 \left(\int_\tau^t \mu(\rho-\tau; \vartheta)d\rho \right)^2 + \sigma_2^2(t-\tau) \right]^3}} \\ &\quad \times \left[(w-x_\tau) \left(\sigma_{2r}^2 \left(\int_\tau^t \mu(\rho-\tau; \vartheta)d\rho \right)^2 + \sigma_2^2(t-\tau) \right) \right. \\ &\quad \left. - \left(\int_\tau^t \mu(\rho-\tau; \vartheta)d\rho - (t-\tau)\mu(t-\tau; \vartheta) \right) \right. \\ &\quad \left. \times \left((w-x_\tau)\sigma_{2r}^2 \int_\tau^t \mu(\rho-\tau; \vartheta)d\rho + \lambda_{2r}\sigma_2^2(t-\tau) \right) \right] \\ &\quad \times \exp \left[-\frac{\left(w-x_\tau-\lambda_{2r} \int_\tau^t \mu(\rho-\tau; \vartheta)d\rho \right)^2}{2 \left(\sigma_{2r}^2 \left(\int_\tau^t \mu(\rho-\tau; \vartheta)d\rho \right)^2 + \sigma_2^2(t-\tau) \right)} \right] \end{aligned} \quad (46)$$

In this way, the proof has been completed.

APPENDIX B

PROOF OF EQUATIONS (11),(12)

When $t > \tau$, based on the law of total probability, the PDF of the lifetime can be formulated as Equation (47) at the bottom of the next page.

To facilitate the calculation of Equation (47), the following parameter simplification definition is provided.

$$\begin{aligned} A &= \sqrt{2\pi(t-\tau)^2 \left[\sigma_{2r}^2 \left(\int_\tau^t \mu(\rho-\tau; \vartheta)d\rho \right)^2 + \sigma_2^2(t-\tau) \right]}, \\ B &= (w-x_\tau)(t-\tau) \left(\sigma_2^2 + \sigma_{2r}^2 \mu(t-\tau; \vartheta) \int_\tau^t \mu(\rho-\tau; \vartheta)d\rho \right), \\ C &= (t-\tau)\sigma_2^2 \\ &\quad \left(\lambda_{2r} \int_\tau^t \mu(\rho-\tau; \vartheta)d\rho - \lambda_{2r}(t-\tau)\mu(t-\tau; \vartheta) \right), \\ D &= \sigma_{2r}^2 \left(\int_\tau^t \mu(\rho-\tau; \vartheta)d\rho \right)^2 + \sigma_2^2(t-\tau), \\ E &= \exp \left[-\frac{\left(w-x_\tau-\lambda_{2r} \int_\tau^t \mu(\rho-\tau; \vartheta)d\rho \right)^2}{2 \left(\sigma_{2r}^2 \left(\int_\tau^t \mu(\rho-\tau; \vartheta)d\rho \right)^2 + \sigma_2^2(t-\tau) \right)} \right], \\ F &= \exp \left[-\frac{(x_\tau-\lambda_{1r}\tau)}{2(\tau\sigma_1^2 + \tau^2\sigma_{1r}^2)} \right], \end{aligned}$$

$$\begin{aligned}
 G &= \sqrt{2\pi(\tau\sigma_1^2 + \tau^2\sigma_{1r}^2)}, \\
 H &= \exp\left(\frac{2\lambda_{1r}w}{\sigma_1^2} + \frac{2(w^2\sigma_{1r}^4\tau + w^2\sigma_{1r}^2\sigma_1^2)}{(\sigma_1^2 + \tau\sigma_{1r}^2)\sigma_1^4}\right) \times \exp\left[-\frac{\left(x_\tau - 2w - \lambda_{1r}\tau - \frac{2w\sigma_{1r}^2\tau}{\sigma_1^2}\right)^2}{2(\tau\sigma_1^2 + \tau^2\sigma_{1r}^2)}\right] \quad (48)
 \end{aligned}$$

$$\begin{aligned}
 f_T(t) &\cong \int_{-\infty}^w f_T(t|x_\tau, \lambda_2)h_\tau(x_\tau|\lambda_{1r}, \sigma_{1r})dx_\tau \\
 &\cong \int_{-\infty}^w \left\{ \frac{1}{\sqrt{2\pi(t-\tau)^2\left[\sigma_{2r}^2\left(\int_\tau^t \mu(\rho-\tau; \vartheta)d\rho\right)^2 + \sigma_2^2(t-\tau)\right]^3}} \right. \\
 &\quad \times \left[(w-x_\tau)\left(\sigma_{2r}^2\left(\int_\tau^t \mu(\rho-\tau; \vartheta)d\rho\right)^2 + \sigma_2^2(t-\tau)\right) \right. \\
 &\quad \left. - \left(\int_\tau^t \mu(\rho-\tau; \vartheta)d\rho - (t-\tau)\mu(t-\tau; \vartheta)\right) \right. \\
 &\quad \left. \times \left((w-x_\tau)\sigma_{2r}^2 \int_\tau^t \mu(\rho-\tau; \vartheta)d\rho + \lambda_{2r}\sigma_2^2(t-\tau)\right) \right] \\
 &\quad \times \exp\left[-\frac{\left(w-x_\tau - \lambda_{2r} \int_\tau^t \mu(\rho-\tau; \vartheta)d\rho\right)^2}{2\left(\sigma_{2r}^2\left(\int_\tau^t \mu(\rho-\tau; \vartheta)d\rho\right)^2 + \sigma_2^2(t-\tau)\right)}\right] \\
 &\quad \times h_\tau(x_\tau|\lambda_{1r}, \sigma_{1r}) \left. \right\} dx_\tau \\
 &\cong \int_{-\infty}^w \left\{ \frac{1}{\sqrt{2\pi(t-\tau)^2\left[\sigma_{2r}^2\left(\int_\tau^t \mu(\rho-\tau; \vartheta)d\rho\right)^2 + \sigma_2^2(t-\tau)\right]}} \right. \\
 &\quad \times \left[\frac{(w-x_\tau)(t-\tau)\left(\sigma_2^2 + \sigma_{2r}^2\mu(t-\tau; \vartheta) \int_\tau^t \mu(\rho-\tau; \vartheta)d\rho\right)}{\sigma_{2r}^2\left(\int_\tau^t \mu(\rho-\tau; \vartheta)d\rho\right)^2 + \sigma_2^2(t-\tau)} \right. \\
 &\quad \left. - \frac{(t-\tau)\sigma_2^2\left(\lambda_{2r} \int_\tau^t \mu(\rho-\tau; \vartheta)d\rho - \lambda_{2r}(t-\tau)\mu(t-\tau; \vartheta)\right)}{\sigma_{2r}^2\left(\int_\tau^t \mu(\rho-\tau; \vartheta)d\rho\right)^2 + \sigma_2^2(t-\tau)} \right] \\
 &\quad \times \exp\left[-\frac{\left(w-x_\tau - \lambda_{2r} \int_\tau^t \mu(\rho-\tau; \vartheta)d\rho\right)^2}{2\left(\sigma_{2r}^2\left(\int_\tau^t \mu(\rho-\tau; \vartheta)d\rho\right)^2 + \sigma_2^2(t-\tau)\right)}\right] \\
 &\quad \times \left[\frac{\exp\left(-\frac{(x_\tau-\lambda_{1r}\tau)}{2(\tau\sigma_1^2 + \tau^2\sigma_{1r}^2)}\right)}{\sqrt{2\pi(\tau\sigma_1^2 + \tau^2\sigma_{1r}^2)}} - \frac{\exp\left(\frac{2\lambda_{1r}w}{\sigma_1^2} + \frac{2(w^2\sigma_{1r}^4\tau + w^2\sigma_{1r}^2\sigma_1^2)}{(\sigma_1^2 + \tau\sigma_{1r}^2)\sigma_1^4}\right)}{\sqrt{2\pi(\tau\sigma_1^2 + \tau^2\sigma_{1r}^2)}} \right. \\
 &\quad \left. \times \exp\left(-\frac{\left(x_\tau - 2w - \lambda_{1r}\tau - \frac{2w\sigma_{1r}^2\tau}{\sigma_1^2}\right)^2}{2(\tau\sigma_1^2 + \tau^2\sigma_{1r}^2)}\right) \right] \left. \right\} dx_\tau \quad (47)
 \end{aligned}$$

Then, Equation (47) could be rewritten as:

$$f_T(t) \cong \int_{-\infty}^w \left\{ \left[\frac{1}{A} \times \left(\frac{B}{D} - \frac{C}{D} \right) \times E \right] \times \left(\frac{F}{G} - \frac{H}{G} \right) \right\} dx_\tau \cong Q - R \quad (49)$$

where $Q = Q_1 - Q_2$, $R = R_1 - R_2$, and

$$\begin{aligned} Q_1 &= \frac{1}{G} \int_{-\infty}^w \left(\frac{1}{A} \times \frac{B}{D} \times E \times F \right) dx_\tau, \\ Q_2 &= \frac{1}{G} \int_{-\infty}^w \left(\frac{1}{A} \times \frac{C}{D} \times E \times F \right) dx_\tau, \\ R_1 &= \frac{1}{G} \int_{-\infty}^w \left(\frac{1}{A} \times \frac{B}{D} \times E \times H \right) dx_\tau, \\ R_2 &= \frac{1}{G} \int_{-\infty}^w \left(\frac{1}{A} \times \frac{C}{D} \times E \times H \right) dx_\tau \end{aligned}$$

To conduct the above integral, Lemma 3 [36] is introduced.

Lemma 3: If y is a Gaussian random variable following $N(\lambda_d, \sigma_d^2)$, then the definite integral of its function $\exp\left[-\frac{(y-\lambda_c)^2}{2\sigma_c^2}\right]$ and $y \exp\left[-\frac{(y-\lambda_c)^2}{2\sigma_c^2}\right]$ hold the following forms,

$$\int_{-\infty}^w \exp\left[-\frac{(y-\lambda_c)^2}{2\sigma_c^2}\right] \frac{1}{\sqrt{2\pi\sigma_d^2}} \exp\left[-\frac{(y-\lambda_d)^2}{2\sigma_d^2}\right] dy = J(1 - \Phi(-K)) \quad (50)$$

$$\int_{-\infty}^w y \exp\left[-\frac{(y-\lambda_c)^2}{2\sigma_c^2}\right] \frac{1}{\sqrt{2\pi\sigma_d^2}} \exp\left[-\frac{(y-\lambda_d)^2}{2\sigma_d^2}\right] dy = J \left(\frac{\lambda_d\sigma_c^2 + \lambda_c\sigma_d^2}{\sigma_c^2 + \sigma_d^2} \Phi(K) - \sqrt{\frac{\sigma_c^2\sigma_d^2}{\sigma_c^2 + \sigma_d^2}} \phi(K) \right) \quad (51)$$

where

$$\begin{aligned} J &= \sqrt{\frac{\sigma_c^2}{\sigma_c^2 + \sigma_d^2}} \exp\left[-\frac{(\lambda_c - \lambda_d)^2}{2(\sigma_c^2 + \sigma_d^2)}\right], \\ K &= \frac{w(\sigma_c^2 + \sigma_d^2) - \lambda_d\sigma_c^2 - \lambda_c\sigma_d^2}{\sqrt{\sigma_c^2\sigma_d^2(\sigma_c^2 + \sigma_d^2)}} \end{aligned}$$

It is worth noting that $\Phi(\cdot)$ and $\phi(\cdot)$ denote the CDF and PDF of the standard normal distribution, respectively.

Then, the analytical results of Equations (11) and (12) in Section II-B-2) could be obtained by calculating Equation (49) based on Lemma 3.

In this way, the proof has been completed.

APPENDIX C PROOF OF EQUATIONS (24),(25)

According to the EM algorithm, the parameter estimation procedure is composed of the following two steps.

E-step: Calculating the conditional expectation $Q(\Theta|\hat{\Theta}^{(k)})$.

$$\begin{aligned} Q(\Theta|\hat{\Theta}^{(k)}) &= E_{Y|X, \hat{\Theta}^{(k)}}[\ln L(\Theta|X, Y)] \end{aligned}$$

$$\begin{aligned} &= \sum_{n=1}^N E_{Y|X, \hat{\Theta}^{(k)}} [\ln (p(Y_n|\Theta)p(X_n|Y_n, \Theta))] \\ &= \sum_{n=1}^N E_{Y|X, \hat{\Theta}^{(k)}} \ln \left\{ \frac{1}{\sqrt{2\pi\sigma_{1r}^2}} \exp\left[-\frac{(\lambda_{1,n} - \lambda_{1r})^2}{2\sigma_{1r}^2}\right] \right. \\ &\quad \times \prod_{j=1}^{\tilde{\tau}_n} \frac{1}{\sqrt{2\pi\sigma_1^2\Delta t}} \exp\left[-\frac{(\Delta x_{n,j} - \lambda_{1,n}\Delta t)^2}{2\sigma_1^2\Delta t}\right] \\ &\quad \times \frac{1}{\sqrt{2\pi\sigma_{2r}^2}} \exp\left[-\frac{(\lambda_{2,n} - \lambda_{2r})^2}{2\sigma_{2r}^2}\right] \prod_{j=\tilde{\tau}_n+1}^{m_n} \frac{1}{\sqrt{2\pi\sigma_2^2\Delta t}} \\ &\quad \left. \times \exp\left[-\frac{(\Delta x_{n,j} - \lambda_{2,n} \int_{t_{j-1}}^{t_j} \mu(\rho - \tau_n; \vartheta)d\rho)^2}{2\sigma_2^2\Delta t}\right] \right\} \quad (52) \end{aligned}$$

To calculate the above-presented equation, the posterior distribution of random variables $\lambda_{1,n}$ and $\lambda_{2,n}$ need to be solved first. Given the observations X_n and the parameter estimates $\hat{\Theta}^{(k)}$ in the k -th iteration, the posterior distributions

of $\lambda_{1,n}$ and $\lambda_{2,n}$ still follow the normal distribution, and could be formulated according to the Bayesian rule.

$$p(Y_n|X_n, \Theta^{(k)}) \propto p(X_n|Y_n, \Theta^{(k)})p(Y_n|\Theta^{(k)}) \quad (53)$$

where $Y_n = \{\lambda_{1,n}, \lambda_{2,n}\}$. Thus, based on the property of the normal distribution for the Bayesian rule, the conditional probability $p(\lambda_{1,n}|X_n, \Theta^{(k)})$ and $p(\lambda_{2,n}|X_n, \Theta^{(k)})$ could be obtained as follows,

$$\begin{aligned} p(\lambda_{1,n}|X_n, \Theta^{(k)}) &= \frac{1}{\sqrt{2\pi} \frac{\hat{\sigma}_{1r}^{2,(k)} \hat{\sigma}_1^{2,(k)} \Delta t}{\tilde{\tau}_n \hat{\sigma}_{1r}^{2,(k)} \Delta t^2 + \hat{\sigma}_1^{2,(k)} \Delta t}} \\ &\quad \times \exp\left[-\frac{\left(\lambda_{1,n} - \frac{(x_n \tilde{\tau}_n - x_{n,0}) \Delta t \hat{\sigma}_{1r}^{2,(k)} + \hat{\sigma}_1^{2,(k)} \Delta t \hat{\lambda}_{1r}^{(k)}}{\tilde{\tau}_n \hat{\sigma}_{1r}^{2,(k)} \Delta t^2 + \hat{\sigma}_1^{2,(k)} \Delta t}\right)^2}{\frac{2\hat{\sigma}_{1r}^{2,(k)} \hat{\sigma}_1^{2,(k)} \Delta t}{\tilde{\tau}_n \hat{\sigma}_{1r}^{2,(k)} \Delta t^2 + \hat{\sigma}_1^{2,(k)} \Delta t}}\right] \quad (54) \end{aligned}$$

$$\begin{aligned} p(\lambda_{2,n}|X_n, \Theta^{(k)}) &= \frac{1}{\sqrt{2\pi N}} \exp\left\{-\frac{[\lambda_{2,n} - M]^2}{2N}\right\} \quad (55) \end{aligned}$$

where

$$\begin{aligned} M &= \frac{\hat{\sigma}_{2r}^{2,(k)} \sum_{j=\tilde{\tau}_n+1}^{m_n} \Delta x_{n,j} \int_{t_{j-1}}^{t_j} \mu(\rho - \tau_n; \vartheta)d\rho + \hat{\sigma}_2^{2,(k)} \Delta t \hat{\lambda}_{2r}^{(k)}}{\hat{\sigma}_{2r}^{2,(k)} \sum_{j=\tilde{\tau}_n+1}^{m_n} \left(\int_{t_{j-1}}^{t_j} \mu(\rho - \tau_n; \vartheta)d\rho\right)^2 + \hat{\sigma}_2^{2,(k)} \Delta t} \\ N &= \frac{\hat{\sigma}_{2r}^{2,(k)} \hat{\sigma}_2^{2,(k)} \Delta t}{\hat{\sigma}_{2r}^{2,(k)} \sum_{j=\tilde{\tau}_n+1}^{m_n} \left(\int_{t_{j-1}}^{t_j} \mu(\rho - \tau_n; \vartheta)d\rho\right)^2 + \hat{\sigma}_2^{2,(k)} \Delta t} \end{aligned}$$

Then, we can attain $\lambda_{1,n}$, $\lambda_{1,n}^2$ and $\lambda_{2,n}$, $\lambda_{2,n}^2$ as follows,

$$\begin{aligned}
 & E[\lambda_{1,n}|X_n, \hat{\Theta}^{(k)}] \\
 &= \frac{(x_n, \tilde{\tau}_n - x_n, 0)\Delta t \hat{\sigma}_{1r}^{2,(k)} + \hat{\sigma}_1^{2,(k)} \Delta t \hat{\lambda}_{1r}^{(k)}}{\tilde{\tau}_n \hat{\sigma}_{1r}^{2,(k)} \Delta t^2 + \hat{\sigma}_1^{2,(k)} \Delta t} \\
 & E[\lambda_{1,n}^2|X_n, \hat{\Theta}^{(k)}] \\
 &= \frac{\hat{\sigma}_{1r}^{2,(k)} \hat{\sigma}_1^{2,(k)} \Delta t}{\tilde{\tau}_n \hat{\sigma}_{1r}^{2,(k)} \Delta t^2 + \hat{\sigma}_1^{2,(k)} \Delta t} \\
 &+ \left[\frac{(x_n, \tilde{\tau}_n - x_n, 0)\Delta t \hat{\sigma}_{1r}^{2,(k)} + \hat{\sigma}_1^{2,(k)} \Delta t \hat{\lambda}_{1r}^{(k)}}{\tilde{\tau}_n \hat{\sigma}_{1r}^{2,(k)} \Delta t^2 + \hat{\sigma}_1^{2,(k)} \Delta t} \right]^2 \\
 & E[\lambda_{2,n}|X_n, \hat{\Theta}^{(k)}] \\
 &= \frac{\hat{\sigma}_{2r}^{2,(k)} \sum_{j=\tilde{\tau}_n+1}^{m_n} \Delta x_{n,j} \int_{t_{j-1}}^{t_j} \mu(\rho - \tau_n; \vartheta) d\rho + \hat{\sigma}_2^{2,(k)} \Delta t \hat{\lambda}_{2r}^{(k)}}{\hat{\sigma}_{2r}^{2,(k)} \sum_{j=\tilde{\tau}_n+1}^{m_n} \left(\int_{t_{j-1}}^{t_j} \mu(\rho - \tau_n; \vartheta) d\rho \right)^2 + \hat{\sigma}_2^{2,(k)} \Delta t} \\
 & E[\lambda_{2,n}^2|X_n, \hat{\Theta}^{(k)}] \\
 &= \frac{\hat{\sigma}_{2r}^{2,(k)} \sum_{j=\tilde{\tau}_n+1}^{m_n} \left(\int_{t_{j-1}}^{t_j} \mu(\rho - \tau_n; \vartheta) d\rho \right)^2 + \hat{\sigma}_2^{2,(k)} \Delta t}{\hat{\sigma}_{2r}^{2,(k)} \sum_{j=\tilde{\tau}_n+1}^{m_n} \Delta x_{n,j} \int_{t_{j-1}}^{t_j} \mu(\rho - \tau_n; \vartheta) d\rho + \hat{\sigma}_2^{2,(k)} \Delta t \hat{\lambda}_{2r}^{(k)}} \left[\frac{\hat{\sigma}_{2r}^{2,(k)} \sum_{j=\tilde{\tau}_n+1}^{m_n} \left(\int_{t_{j-1}}^{t_j} \mu(\rho - \tau_n; \vartheta) d\rho \right)^2 + \hat{\sigma}_2^{2,(k)} \Delta t}{\hat{\sigma}_{2r}^{2,(k)} \sum_{j=\tilde{\tau}_n+1}^{m_n} \Delta x_{n,j} \int_{t_{j-1}}^{t_j} \mu(\rho - \tau_n; \vartheta) d\rho + \hat{\sigma}_2^{2,(k)} \Delta t \hat{\lambda}_{2r}^{(k)}} \right]^2
 \end{aligned} \tag{56}$$

Based on Equation (56), the conditional expectation $Q(\Theta|\hat{\Theta}^{(k)})$ in Equation (52) could be calculated as follows,

$$\begin{aligned}
 & Q(\Theta|\hat{\Theta}^{(k)}) \\
 &= \left\{ n \ln \frac{1}{\sqrt{2\pi\sigma_{1r}^2}} - \frac{\sum_{n=1}^N \varphi_1^{2,(k)} - 2\lambda_{1r} \sum_{n=1}^N \varphi_1^{(k)} + n\lambda_{1r}^2}{2\sigma_{1r}^2} \right. \\
 &+ \sum_{n=1}^N \tilde{\tau}_n \ln \frac{1}{\sqrt{2\pi\sigma_1^2 \Delta t}} \\
 &\left. - \sum_{n=1}^N \frac{\sum_{j=1}^{\tilde{\tau}_n} \Delta x_{n,j}^2 - 2\varphi_1^{(k)} \sum_{j=1}^{\tilde{\tau}_n} \Delta x_{n,j} \Delta t + \tilde{\tau}_n \varphi_1^{2,(k)} \Delta t^2}{2\sigma_1^2 \Delta t} \right\} \\
 &+ \left\{ n \ln \frac{1}{\sqrt{2\pi\sigma_{2r}^2}} - \frac{\sum_{n=1}^N \varphi_2^{2,(k)} - 2\lambda_{2r} \sum_{n=1}^N \varphi_2^{(k)} + n\lambda_{2r}^2}{2\sigma_{2r}^2} \right. \\
 &\left. + \sum_{n=1}^N (m_n - \tilde{\tau}_n) \ln \frac{1}{\sqrt{2\pi\sigma_2^2 \Delta t}} \right\}
 \end{aligned}$$

$$\left. - \sum_{n=1}^N \frac{\sum_{j=\tilde{\tau}_n+1}^{m_n} \Delta x_{n,j}^2 - 2\varphi_2^{(k)} \sum_{j=\tilde{\tau}_n+1}^{m_n} \Delta x_{n,j} \eta(t_j) + \varphi_2^{2,(k)} \sum_{j=\tilde{\tau}_n+1}^{m_n} \eta^2(t_j)}{2\sigma_2^2 \Delta t} \right\} \tag{57}$$

where

$$\begin{aligned}
 \varphi_1^{(k)} &= E[\lambda_{1,n}|X_n, \hat{\Theta}^{(k)}], \varphi_1^{2,(k)} = E[\lambda_{1,n}^2|X_n, \hat{\Theta}^{(k)}], \\
 \varphi_2^{(k)} &= E[\lambda_{2,n}|X_n, \hat{\Theta}^{(k)}], \varphi_2^{2,(k)} = E[\lambda_{2,n}^2|X_n, \hat{\Theta}^{(k)}], \\
 \eta(t_j) &= \int_{t_{j-1}}^{t_j} \mu(\rho - \tau_n; \vartheta) d\rho
 \end{aligned}$$

M-step : Computing $\hat{\Theta}^{(k+1)}$ by maximizing $Q(\Theta|\hat{\Theta}^{(k)})$ with respect to Θ .

After obtaining $Q(\Theta|\hat{\Theta}^{(k)})$, the unknown parameters $\hat{\Theta}^{(k+1)}$ could be obtained by calculating $\partial Q(\Theta|\hat{\Theta}^{(k)})/\partial \Theta = 0$. However, the above results of $Q(\Theta|\hat{\Theta}^{(k)})$ are affected by the nonlinear drift function involved by the parameter ϑ . Hence, it is difficult to obtain $\hat{\Theta}^{(k+1)}$ through maximizing Equation (57) directly. Here, $\hat{\Theta}^{(k+1)}$ is calculated by the profile log-likelihood function method, which is similar to the procedure proposed in Section II-C-1). The detailed steps are as follows.

Firstly, given ϑ , the results of $\hat{\Theta}^{(k+1)}$ in the $(k+1)$ -th step could be obtained as follows (58), shown at the top of the next page, where $\varphi_1^{(k)}$, $\varphi_1^{2,(k)}$, $\varphi_2^{(k)}$, $\varphi_2^{2,(k)}$, $\eta(t_j)$ has been defined in Equations (56) and (57).

It can be found in Equation (58) that if $\hat{\Theta}^{(k)}$ is given, $\hat{\lambda}_{1r}^{(k+1)}$, $\hat{\sigma}_{1r}^{(k+1)}$ and $\hat{\sigma}_1^{(k+1)}$ are independent of ϑ , which means that their results in Equation (58) are the optimal estimates in the $(k+1)$ -th step. However, $\hat{\lambda}_{2r}^{(k+1)}(\vartheta)$, $\hat{\sigma}_{2r}^{(k+1)}(\vartheta)$ and $\hat{\sigma}_2^{(k+1)}(\vartheta)$ in Equation (58) are functions of ϑ . Thus, to obtain the final estimates of these three parameters, we need to calculate ϑ first. According to the independent assumption of THDM, the profile log-likelihood function of ϑ could be constructed by substituting the expressions of $\hat{\lambda}_{2r}^{(k+1)}(\vartheta)$, $\hat{\sigma}_{2r}^{(k+1)}(\vartheta)$ and $\hat{\sigma}_2^{(k+1)}(\vartheta)$ into the formulas of the second curly bracket in Equation (57). Due to space limitations, it is omitted here. In this way, the estimate of ϑ in the $(k+1)$ -th step, i.e., $\vartheta^{(k+1)}$, could be obtained by maximizing the profile log-likelihood function based on a search algorithm. Here, the MATLAB function “fminsearch” is utilized for this aim. Then, substituting $\vartheta^{(k+1)}$ into Equation (58), the estimates of $\hat{\lambda}_{2r}^{(k+1)}(\vartheta)$, $\hat{\sigma}_{2r}^{(k+1)}(\vartheta)$ and $\hat{\sigma}_2^{(k+1)}(\vartheta)$ in the $(k+1)$ -th step could be derived, respectively. Through this procedure, all parameters in $(k+1)$ -th could be obtained.

It is noteworthy that after obtaining $\hat{\Theta}^{(k+1)}$, the estimated values of all parameters in the $(k+1)$ -th step including $\vartheta^{(k+1)}$ will be treated as the initial values of the next EM iteration. Thus, the final parameter estimates could be obtained when the convergence criterion is satisfied.

In this way, the proof has been completed.

$$\begin{aligned}
\hat{\lambda}_{1r}^{(k+1)} &= \frac{1}{N} \sum_{n=1}^N \varphi_1^{(k)}, \hat{\sigma}_{1r}^{(k+1)} = \sqrt{\frac{1}{N} \sum_{n=1}^N \left[\varphi_1^{2,(k)} - 2\varphi_1^{(k)} \hat{\lambda}_{1r}^{(k+1)} + \left(\hat{\lambda}_{1r}^{(k+1)} \right)^2 \right]} \\
\hat{\sigma}_1^{(k+1)} &= \sqrt{\frac{\sum_{n=1}^N \left[\sum_{j=1}^{\tilde{\tau}_n} \Delta x_{n,j}^2 - 2\varphi_1^{(k)} \sum_{j=1}^{\tilde{\tau}_n} \Delta x_{n,j} \Delta t + \tilde{\tau}_n \varphi_1^{2,(k)} \Delta t^2 \right]}{\sum_{n=1}^N \tilde{\tau}_n \Delta t}} \\
\hat{\lambda}_{2r}^{(k+1)} &= \frac{1}{N} \sum_{n=1}^N \varphi_2^{(k)} \\
\hat{\sigma}_{2r}^{(k+1)} &= \sqrt{\frac{1}{N} \sum_{n=1}^N \left[\varphi_2^{2,(k)} - 2\varphi_2^{(k)} \hat{\lambda}_{2r}^{(k+1)} + \left(\hat{\lambda}_{2r}^{(k+1)} \right)^2 \right]} \\
\hat{\sigma}_2^{(k+1)} &= \sqrt{\frac{\sum_{n=1}^N \left[\sum_{j=\tilde{\tau}_n+1}^{m_n} \Delta x_{n,j}^2 - 2\varphi_2^{(k)} \sum_{j=\tilde{\tau}_n+1}^{m_n} \Delta x_{n,j} \eta(t_j) + \varphi_2^{2,(k)} \sum_{j=\tilde{\tau}_n+1}^{m_n} \eta^2(t_j) \right]}{\sum_{n=1}^N (m_n - \tilde{\tau}_n) \Delta t}} \quad (58)
\end{aligned}$$

REFERENCES

- [1] F.-K. Wang and T. Mamo, "A hybrid model based on support vector regression and differential evolution for remaining useful lifetime prediction of lithium-ion batteries," *J. Power Sources*, vol. 401, pp. 49–54, Oct. 2018.
- [2] X. Hu, L. Xu, X. Lin, and M. Pecht, "Battery lifetime prognostics," *Joule*, vol. 4, no. 2, pp. 310–346, Feb. 2020.
- [3] X. Li, C. Yuan, and Z. Wang, "State of health estimation for Li-ion battery via partial incremental capacity analysis based on support vector regression," *Energy*, vol. 203, Jul. 2020, Art. no. 117852.
- [4] S. Landini and T. S. O'Donovan, "Novel experimental approach for the characterisation of lithium-ion cells performance in isothermal conditions," *Energy*, vol. 214, Jan. 2021, Art. no. 118965.
- [5] X. Li, J. Zhao, J. Duan, S. Panchal, J. Yuan, R. Fraser, M. Fowler, and M. Chen, "Simulation of cooling plate effect on a battery module with different channel arrangement," *J. Energy Storage*, vol. 49, May 2022, Art. no. 104113.
- [6] Y. Song, D. Liu, Y. Hou, J. Yu, and Y. Peng, "Satellite lithium-ion battery remaining useful life estimation with an iterative updated RVM fused with the KF algorithm," *Chin. J. Aeronaut.*, vol. 31, no. 1, pp. 31–40, Jan. 2018.
- [7] B. Liu, Y. Jia, C. Yuan, L. Wang, X. Gao, S. Yin, and J. Xu, "Safety issues and mechanisms of lithium-ion battery cell upon mechanical abusive loading: A review," *Energy Storage Mater.*, vol. 24, pp. 85–112, Jan. 2020.
- [8] R. Xiong, Y. Pan, W. Shen, H. Li, and F. Sun, "Lithium-ion battery aging mechanisms and diagnosis method for automotive applications: Recent advances and perspectives," *Renew. Sustain. Energy Rev.*, vol. 131, Oct. 2020, Art. no. 110048.
- [9] F. Guo, X. Wu, L. Liu, J. Ye, T. Wang, L. Fu, and Y. Wu, "Prediction of remaining useful life and state of health of lithium batteries based on time series feature and Savitzky–Golay filter combined with gated recurrent unit neural network," *Energy*, vol. 270, May 2023, Art. no. 126880.
- [10] F. Wang, Z. Zhao, J. Ren, Z. Zhai, S. Wang, and X. Chen, "A transferable lithium-ion battery remaining useful life prediction method from cycle-consistency of degradation trend," *J. Power Sources*, vol. 521, Feb. 2022, Art. no. 230975.
- [11] S. Atalay, M. Sheikh, A. Mariani, Y. Merla, E. Bower, and W. D. Widanage, "Theory of battery ageing in a lithium-ion battery: Capacity fade, nonlinear ageing and lifetime prediction," *J. Power Sources*, vol. 478, Dec. 2020, Art. no. 229026.
- [12] X. Pang, Z. Zhao, J. Wen, J. Jia, Y. Shi, J. Zeng, and Y. Dong, "An interval prediction approach based on fuzzy information granulation and linguistic description for remaining useful life of lithium-ion batteries," *J. Power Sources*, vol. 542, Sep. 2022, Art. no. 231750.
- [13] Y. H. Lui, M. Li, A. Downey, S. Shen, V. P. Nemani, H. Ye, C. Van Elzen, G. Jain, S. Hu, S. Laflamme, and C. Hu, "Physics-based prognostics of implantable-grade lithium-ion battery for remaining useful life prediction," *J. Power Sources*, vol. 485, Feb. 2021, Art. no. 229327.
- [14] Y. Jiang, Y. Chen, F. Yang, and W. Peng, "State of health estimation of lithium-ion battery with automatic feature extraction and self-attention learning mechanism," *J. Power Sources*, vol. 556, Feb. 2023, Art. no. 232466.
- [15] M.-F. Ng, J. Zhao, Q. Yan, G. J. Conduit, and Z. W. Seh, "Predicting the state of charge and health of batteries using data-driven machine learning," *Nature Mach. Intell.*, vol. 2, no. 3, pp. 161–170, Mar. 2020.
- [16] M.-F. Ge, Y. Liu, X. Jiang, and J. Liu, "A review on state of health estimations and remaining useful life prognostics of lithium-ion batteries," *Measurement*, vol. 174, Apr. 2021, Art. no. 109057.
- [17] J. Guo, Z. Li, and M. Li, "A review on prognostics methods for engineering systems," *IEEE Trans. Rel.*, vol. 69, no. 3, pp. 1110–1129, Sep. 2020.
- [18] B. Ma, S. Yang, L. Zhang, W. Wang, S. Chen, X. Yang, H. Xie, H. Yu, H. Wang, and X. Liu, "Remaining useful life and state of health prediction for lithium batteries based on differential thermal voltammetry and a deep-learning model," *J. Power Sources*, vol. 548, Nov. 2022, Art. no. 232030.
- [19] Y. Lei, N. Li, L. Guo, N. Li, T. Yan, and J. Lin, "Machinery health prognostics: A systematic review from data acquisition to RUL prediction," *Mech. Syst. Signal Process.*, vol. 104, pp. 799–834, May 2018.
- [20] Y. Lei, N. Li, and J. Lin, "A new method based on stochastic process models for machine remaining useful life prediction," *IEEE Trans. Instrum. Meas.*, vol. 65, no. 12, pp. 2671–2684, Dec. 2016.
- [21] J.-X. Zhang, D.-B. Du, X.-S. Si, Y. Liu, and C.-H. Hu, "Prognostics based on stochastic degradation process: The last exit time perspective," *IEEE Trans. Rel.*, vol. 70, no. 3, pp. 1158–1176, Sep. 2021.
- [22] S. Zhang, Q. Zhai, X. Shi, and X. Liu, "A Wiener process model with dynamic covariate for degradation modeling and remaining useful life prediction," *IEEE Trans. Rel.*, vol. 72, no. 1, pp. 214–223, Mar. 2023.
- [23] Z. Zhang, X. Si, C. Hu, and Y. Lei, "Degradation data analysis and remaining useful life estimation: A review on Wiener-process-based methods," *Eur. J. Oper. Res.*, vol. 271, no. 3, pp. 775–796, Dec. 2018.

- [24] L. Shen, Y. Wang, Q. Zhai, and Y. Tang, "Degradation modeling using stochastic processes with random initial degradation," *IEEE Trans. Rel.*, vol. 68, no. 4, pp. 1320–1329, Dec. 2019.
- [25] B. Cai, H. Fan, X. Shao, Y. Liu, G. Liu, Z. Liu, and R. Ji, "Remaining useful life re-prediction methodology based on Wiener process: Subsea Christmas tree system as a case study," *Comput. Ind. Eng.*, vol. 151, Jan. 2021, Art. no. 106983.
- [26] X. Xu, S. Tang, C. Yu, J. Xie, X. Han, and M. Ouyang, "Remaining useful life prediction of lithium-ion batteries based on Wiener process under time-varying temperature condition," *Rel. Eng. Syst. Saf.*, vol. 214, Oct. 2021, Art. no. 107675.
- [27] X.-S. Si, W. Wang, C.-H. Hu, M.-Y. Chen, and D.-H. Zhou, "A Wiener-process-based degradation model with a recursive filter algorithm for remaining useful life estimation," *Mech. Syst. Signal Process.*, vol. 35, nos. 1–2, pp. 219–237, Feb. 2013.
- [28] X.-S. Si, W. Wang, C.-H. Hu, and D.-H. Zhou, "Estimating remaining useful life with three-source variability in degradation modeling," *IEEE Trans. Rel.*, vol. 63, no. 1, pp. 167–190, Mar. 2014.
- [29] J. Li, B. Jing, H. Dai, X. Jiao, and X. Liu, "Remaining useful life prediction based on variation coefficient consistency test of a Wiener process," *Chin. J. Aeronaut.*, vol. 31, no. 1, pp. 107–116, Jan. 2018.
- [30] X.-S. Si, W. Wang, C.-H. Hu, D.-H. Zhou, and M. G. Pecht, "Remaining useful life estimation based on a nonlinear diffusion degradation process," *IEEE Trans. Rel.*, vol. 61, no. 1, pp. 50–67, Mar. 2012.
- [31] Z.-X. Zhang, X.-S. Si, and C.-H. Hu, "An Age- and state-dependent nonlinear prognostic model for degrading systems," *IEEE Trans. Rel.*, vol. 64, no. 4, pp. 1214–1228, Dec. 2015.
- [32] X.-S. Si, "An adaptive prognostic approach via nonlinear degradation modeling: Application to battery data," *IEEE Trans. Ind. Electron.*, vol. 62, no. 8, pp. 5082–5096, Aug. 2015.
- [33] H. Zhang, Z. Mo, J. Wang, and Q. Miao, "Nonlinear-drifted fractional Brownian motion with multiple hidden state variables for remaining useful life prediction of lithium-ion batteries," *IEEE Trans. Rel.*, vol. 69, no. 2, pp. 768–780, Jun. 2020.
- [34] Y. Zhang, Y. Yang, H. Li, X. Xiu, and W. Liu, "A data-driven modeling method for stochastic nonlinear degradation process with application to RUL estimation," *IEEE Trans. Syst., Man, Cybern., Syst.*, vol. 52, no. 6, pp. 3847–3858, Jun. 2022.
- [35] W. L. Burgess, "Valve regulated lead acid battery float service life estimation using a Kalman filter," *J. Power Sources*, vol. 191, no. 1, pp. 16–21, Jun. 2009.
- [36] J.-X. Zhang, C.-H. Hu, X. He, X.-S. Si, Y. Liu, and D.-H. Zhou, "A novel lifetime estimation method for two-phase degrading systems," *IEEE Trans. Rel.*, vol. 68, no. 2, pp. 689–709, Jun. 2019.
- [37] D. Kong, N. Balakrishnan, and L. Cui, "Two-phase degradation process model with abrupt jump at change point governed by Wiener process," *IEEE Trans. Rel.*, vol. 66, no. 4, pp. 1345–1360, Dec. 2017.
- [38] H. Gao, L. Cui, and Q. Dong, "Reliability modeling for a two-phase degradation system with a change point based on a Wiener process," *Rel. Eng. Syst. Saf.*, vol. 193, Jan. 2020, Art. no. 106601.
- [39] X. Chen, Z. Liu, J. Wang, C. Yang, B. Long, and X. Zhou, "An adaptive prediction model for the remaining life of an Li-ion battery based on the fusion of the two-phase Wiener process and an extreme learning machine," *Electronics*, vol. 10, no. 5, p. 540, Feb. 2021.
- [40] Y. Zhang, T. Wik, J. Bergström, M. Pecht, and C. Zou, "A machine learning-based framework for online prediction of battery ageing trajectory and lifetime using histogram data," *J. Power Sources*, vol. 526, Apr. 2022, Art. no. 231110.
- [41] K. Gao, J. Xu, Z. Li, Z. Cai, D. Jiang, and A. Zeng, "A novel remaining useful life prediction method for capacity fading lithium-ion batteries," *ACS Omega*, vol. 7, no. 30, pp. 26701–26714, Aug. 2022.
- [42] Z. Fei, Z. Zhang, F. Yang, and K.-L. Tsui, "A deep attention-assisted and memory-augmented temporal convolutional network based model for rapid lithium-ion battery remaining useful life predictions with limited data," *J. Energy Storage*, vol. 62, Jun. 2023, Art. no. 106903.
- [43] M. R. Palacín and A. de Guibert, "Why do batteries fail?" *Science*, vol. 351, no. 6273, Feb. 2016, Art. no. 1253292.
- [44] L. Shen, Y. Zhang, K. Song, and B. Song, "Failure analysis of a lock mechanism with multiple dependent components based on two-phase degradation model," *Eng. Failure Anal.*, vol. 104, pp. 1076–1093, Oct. 2019.
- [45] L. Cui, X. Wang, H. Wang, and J. Ma, "Research on remaining useful life prediction of rolling element bearings based on time-varying Kalman filter," *IEEE Trans. Instrum. Meas.*, vol. 69, no. 6, pp. 2858–2867, Jun. 2020.
- [46] X.-S. Si, T. Li, J. Zhang, and Y. Lei, "Nonlinear degradation modeling and prognostics: A box-cox transformation perspective," *Rel. Eng. Syst. Saf.*, vol. 217, Jan. 2022, Art. no. 108120.
- [47] K. Liu, T. Zou, M. Xin, and C. Lv, "RUL prediction based on two-phase Wiener process," *Qual. Rel. Eng. Int.*, vol. 38, no. 7, pp. 3829–3843, Nov. 2022.
- [48] W.-A. Yan, B.-W. Song, G.-L. Duan, and Y.-M. Shi, "Real-time reliability evaluation of two-phase Wiener degradation process," *Commun. Statist.-Theory Methods*, vol. 46, no. 1, pp. 176–188, Jan. 2017.
- [49] P. Wang, Y. Tang, S. J. Bae, and A. Xu, "Bayesian approach for two-phase degradation data based on change-point Wiener process with measurement errors," *IEEE Trans. Rel.*, vol. 67, no. 2, pp. 688–700, Jun. 2018.
- [50] J. Zhang, X. Si, D. Du, C. Hu, and C. Hu, "Lifetime estimation for multi-phase deteriorating process with random abrupt jumps," *Sensors*, vol. 19, no. 6, p. 1472, Mar. 2019.
- [51] Y. Wen, J. Wu, D. Das, and T.-L. Tseng, "Degradation modeling and RUL prediction using Wiener process subject to multiple change points and unit heterogeneity," *Rel. Eng. Syst. Saf.*, vol. 176, pp. 113–124, Aug. 2018.
- [52] Q. Guan, X. Wei, W. Bai, and L. Jia, "Two-stage degradation modeling for remaining useful life prediction based on the Wiener process with measurement errors," *Qual. Rel. Eng. Int.*, vol. 38, no. 7, pp. 3485–3512, Nov. 2022.
- [53] K. A. Severson, P. M. Attia, N. Jin, N. Perkins, B. Jiang, Z. Yang, M. H. Chen, M. Aykol, P. K. Herring, D. Fraggedakis, M. Z. Bazant, S. J. Harris, W. C. Chueh, and R. D. Braatz, "Data-driven prediction of battery cycle life before capacity degradation," *Nature Energy*, vol. 4, no. 5, pp. 383–391, Mar. 2019.
- [54] A. Molini, P. Talkner, G. G. Katul, and A. Porporato, "First passage time statistics of Brownian motion with purely time dependent drift and diffusion," *Phys. A, Stat. Mech. Appl.*, vol. 390, no. 11, pp. 1841–1852, Jun. 2011.
- [55] Y. Wang, Y. Peng, Y. Zi, X. Jin, and K.-L. Tsui, "A two-stage data-driven-based prognostic approach for bearing degradation problem," *IEEE Trans. Ind. Informat.*, vol. 12, no. 3, pp. 924–932, Jun. 2016.
- [56] X.-S. Si, W. Wang, M.-Y. Chen, C.-H. Hu, and D.-H. Zhou, "A degradation path-dependent approach for remaining useful life estimation with an exact and closed-form solution," *Eur. J. Oper. Res.*, vol. 226, no. 1, pp. 53–66, Apr. 2013.
- [57] Z. Wang, A. Zhang, C. Liu, and Q. Wu, "Reliability analysis for multi-phase Wiener processes considering phase-varying nonlinearity," *IEEE Access*, vol. 8, pp. 223189–223201, 2020.
- [58] X. Hu, Y. Che, X. Lin, and S. Onori, "Battery health prediction using fusion-based feature selection and machine learning," *IEEE Trans. Transport. Electrification*, vol. 7, no. 2, pp. 382–398, Jun. 2021.
- [59] Z. Chen, L. Chen, Z. Ma, K. Xu, Y. Zhou, and W. Shen, "Joint modeling for early predictions of Li-ion battery cycle life and degradation trajectory," *Energy*, vol. 277, Aug. 2023, Art. no. 127633.
- [60] P. Guo, Z. Cheng, and L. Yang, "A data-driven remaining capacity estimation approach for lithium-ion batteries based on charging health feature extraction," *J. Power Sources*, vol. 412, pp. 442–450, Feb. 2019.
- [61] X. Li, L. Zhang, Z. Wang, and P. Dong, "Remaining useful life prediction for lithium-ion batteries based on a hybrid model combining the long short-term memory and Elman neural networks," *J. Energy Storage*, vol. 21, pp. 510–518, Feb. 2019.
- [62] B. Sun, J. Pan, Z. Wu, Q. Xia, Z. Wang, Y. Ren, D. Yang, X. Guo, and Q. Feng, "Adaptive evolution enhanced physics-informed neural networks for time-variant health prognosis of lithium-ion batteries," *J. Power Sources*, vol. 556, Feb. 2023, Art. no. 232432.
- [63] L. Feng, H. Wang, X. Si, and H. Zou, "A state-space-based prognostic model for hidden and age-dependent nonlinear degradation process," *IEEE Trans. Autom. Sci. Eng.*, vol. 10, no. 4, pp. 1072–1086, Oct. 2013.
- [64] W. Zhao, C. Zhang, J. Wang, S. Wang, D. Lv, and F. Qin, "Research on digital twin driven rolling bearing model-data fusion life prediction method," *IEEE Access*, vol. 11, pp. 48611–48627, 2023.
- [65] W. Yu, W. Tu, I. Y. Kim, and C. Mechefske, "A nonlinear-drift-driven Wiener process model for remaining useful life estimation considering three sources of variability," *Rel. Eng. Syst. Saf.*, vol. 212, Aug. 2021, Art. no. 107631.



XUEMIAO CUI received the B.S. degree in vehicle engineering from Henan University of Technology, China, and the M.S. degree in mechanical engineering from Liaoning University of Technology, China. He is currently pursuing the Ph.D. degree in mechanical engineering with Beijing Institute of Technology, China. His research interests include prognostics and health management, reliability estimation, and remaining useful life prediction.



YAFENG HAN received the B.S. and M.S. degrees in mechanical engineering from Beihang University, China, and the Ph.D. degree in mechanical engineering from the National University of Singapore. Since 2019, he has been an Assistant Professor with the School of Mechanical Engineering, Beijing Institute of Technology. His research interests include additive manufacturing, prognostics and health management, equipment integrated logistics support designing, and reliability estimation.

• • •



JIPING LU received the B.S., M.S., and Ph.D. degrees in mechanical engineering from Beijing Institute of Technology, China. Since 2005, he has been a Professor with the School of Mechanical Engineering, Beijing Institute of Technology. His research interests include digital manufacturing, digital twinning technology, big data and knowledge discovery, condition monitoring, prognostics and health management, reliability estimation, and predictive maintenance.